scientific reports

Check for updates

OPEN

Proteomic mechanism of sugar and organic acid metabolism during Korla fragrant pear (*Pyrus sinkiangensis* Yü) fruit development

Yi Wang[1,2,3]✉, Yonghui Deng[1,3], Wei Jiang[2], Shijie An[1], Ling Ma[1], Zhendong Wang[1], Qiangqing Zheng[1], Pan Yan[1]✉ & Qiling Chen[1]✉

Korla fragrant pear (*Pyrus sinkiangensis* Yü) fruit development involves complex physiological and biochemical processes; however, few data are available at the proteomic and metabolomic levels, which would be helpful for understanding the molecular mechanisms of fruit and quality development. Here, Korla fragrant pear was investigated across three stages, namely, early development (5 weeks after flower blooming, WAF), middle development (10WAF), and near ripening (15WAF), via tandem mass tag (TMT) labeling technology and ultra-performance liquid chromatography–tandem mass spectrometry (UPLC–MS/MS). Through proteomic and metabolomic analyses, we identified a total of 8487 proteins expressed during pear fruit development, and 3762 differentially expressed proteins (DEPs) were characterized at three fruit development stages. Moreover, 27 soluble sugars and 43 organic acids were found to accumulate differentially in the fruit at different developmental stages. The expression of proteins related to sugar metabolism and accumulation increased with increasing fruit development stage, which was consistent with the trend in soluble sugar content during fruit development. All 6 disaccharides, including cellobiose (Cel), lactose (Lac), maltose (Mal), trehalose (Tre), phenylglucoside (Phe) and sucrose (Suc), detected in this study were present at low levels in the early stages of fruit development but accumulated in large amounts from 15 WAF to 20 WAF, which may explain the high sweetness of the ripe Korla fragrant pear. In addition, The low organic acid levels during fruit development may explain the low organic acid content of Korla fragrant pear. Thus, our proteomic and metabolomic analyses reveal the molecular basis for the high sweetness and the low organic acidity of Korla fragrant pears.

Keywords *Pyrus sinkiangensis* Yü, Proteomic mechanism, Soluble sugars, Organic acids, Fruit development

Pyrus sinkiangensis Yü is an economically unique forest tree species found in China; it is a high-quality, characteristic fruit tree species that has been planted on a large scale and is distributed primarily across the southern Xinjiang region[1,2]. The fruit of *P. sinkiangensis* Yü is rich in nutrients, such as polysaccharides, phenolic compounds, and vitamins, and it contains a variety of mineral elements, giving it free radical scavenging, anti-inflammatory, and antipyretic pharmacological effects[3,4]. Because of its thin skin, crisp flesh, high sugar content, and rich aroma, the Korla fragrant pear is very popular among consumers on the market[4–6]. Compared with other major pear varieties found in China (such as white pear, autumn pear, sand pear, western pear, etc.), the Korla fragrant pear has excellent qualities, including thin skin and juicy, tender flesh, fewer dregs and a beautiful taste, and the fructose and glucose contents of the Korla fragrant pear are greater than those of the common pear[7]. Moreover, the sorbitol and sucrose contents are similar to those of the white pear[7,8].

Some relevant studies suggest that Korla fragrant pear fruits typically mature between 60 and 140 days after flowering. During fruit development, the growth dynamic curve of the pear fruits is a “double S” shape, with the increase in both diameters divided into three stages: a rapid growth period, a slow growth period, and a preripening rapid growth period, with a trend of "fast—slow—fast – slow[9,10]." A comprehensive understanding

[1]Xinjiang Production and Construction Corps, Key Laboratory of Korla Fragrant Pear Germplasm Innovation and Quality Improvement and Efficiency Increment, Tiemenguan Experimental Station, Xinjiang Academy of Agricultural and Reclamation Sciences, Tiemenguan 841000, China. [2]College of Horticulture and Landscape Architecture, Zhongkai University of Agriculture and Engineering, Guangzhou 510225, China. [3]Yi Wang and Yonghui Deng contributed equally to this work. ✉email: wangyi@zhku.edu.cn; yanpan11235@163.com; cql619@163.com

of genetic elements is important for understanding the regulation of fruit development[11]. Although the pathways involved in the biological process of Korla fragrant pear fruit development and ripening are complex and usually include integrated metabolic changes, many studies have investigated pear-related traits such as the formation of stone cells[12,13], sugar accumulation[14], and organic acid metabolism[15]. Research has shown that the organic acid content of the balsam pear is relatively low compared with that of other pear varieties and that the main organic acid is malic acid[7]. The sugar-to-organic acid content ratio of the Korla fragrant pear is similar to that of the autumn pear and significantly greater than that of the white pear, autumn pear, western pear, or other major pear plant varieties. Therefore, the high sweetness and low organic acid content of the Korla fragrant pear are the key characteristics that distinguish it from other pear varieties[14]. Following the application of molecular biotechnology to pear research, several genes involved in biological pathways have been identified and successfully cloned. For example, the gene encoding soluble acid invertase, which plays an important role in the accumulation of hexoses during fruit enlargement, has been cloned[16,17]. The gene encoding cinnamoyl coenzyme reductase (CCR) is involved in regulating lignin biosynthesis in pear fruits and plays an important role in the formation of stone cells in pear pulp[18]. It has been demonstrated that during the development of Japanese pears, ethylene levels are regulated by the gene encoding 1-aminocyclopropane-1-carboxylate synthase[19]. However, it is still difficult to elucidate broader patterns of genetic control and to identify the key genes responsible for fruit development via partial biosynthesis, which encompasses only a few known genes.

In previous studies, proteomics has been shown to be a powerful approach for establishing functional correlations between phenotypes and genotypes and for characterizing biochemical networks[17,18,20,21], such as studies regarding the development of fruits by strawberry[19,22], mango[20,23], palm[21,24], watermelon[22,25], and papaya plants[23,26]. Proteomics is an extremely favorable tool for studying fruit growth and development, and it can not only reveal the molecular mechanism of fruit tree growth and development but also improve the efficiency of fruit tree breeding[27]. An investigation on the protein expression profiles of Korla fragrant pears during cold storage revealed 21 differentially expressed proteins involved primarily in carbohydrate and energy metabolism, responses to storage environment stimuli and protein metabolism and revealed that these metabolic pathways may individually or collectively regulate the response of balsam pears to cold storage[25,28]. A study using 'Cuiguan' pears as a test material revealed metabolic changes in the kernel and mesocarp during fruit ripening, indicating that the kernel had relatively more titratable acid but lower total soluble solids and that the kernel had a higher citric acid content than the mesocarp during ripening[28]. However, data concerning the protein composition of Korla fragrant pear during fruit development are very limited, and the proteomic mechanism of sugar accumulation in Korla fragrant pear fruits is unclear. Tandem mass tag (TMT) labeling technology is a powerful proteomics technique with high accuracy and sensitivity, demonstrating a remarkable advantage in the simultaneous analysis of multiple samples and subsequently providing relative quantification for hundreds of proteins at one time[21,29]. The TMT technique can produce high-quality and reproducible results in terms of plant growth and development and the response to biotic and abiotic stresses. Therefore, TMT technology has been widely used in the study of plant proteomics[21,30].

However, functional genomic research has confirmed that information garnered from nucleotide data does not necessarily match the corresponding translated protein sequence in an accurate physiological manner[31]. As molecules that directly influence biological processes, proteins have their own special activity patterns, and information at the gene transcription level is not sufficient to reveal the exact functions of intracellular processes. In this study, we used TMT-based quantitative proteomics technology to identify and compare the protein expression characteristics of the Korla fragrant pear at different developmental stages via liquid chromatography–tandem mass spectrometry (LC–MS/MS) and to screen key differentially expressed proteins associated with balsam pear fruit development to reveal the molecular mechanism of Korla fragrant pear development at the protein expression level and provide a theoretical basis for improving the fruit quality of the balsam pear.

Results

Protein identification and quantification

TMT-based quantitative proteomic analysis was performed to analyze the dynamic changes in protein expression in the Korla fragrant pear at 5 WAF, 10 WAF and 15 WAF (Fig. 1). A total of 388901 spectra were obtained, 102861 of which were the matched peptide spectra. A total of 36418 unique peptides were obtained, and we identified a total of 8487 proteins (IPs) (Table 1). A PCA of the IPs revealed that using three biological replicates per group yielded good repeatability, indicating the high quality of the data for effective statistical analysis (Fig. 2).

Quality control of MS data

High-quality mass spectrometry (MS) data are the first step in obtaining reliable proteomics results. In this study, we conducted a sample correlation analysis for the identified proteins, measuring the correlation between samples, and it reflected a good correlation among the samples (Fig. 3A). Moreover, we visualized the distribution of the expression levels of the identified proteins and found that there was a strong correlation within the groups, with the data being more concentrated within the groups (Fig. 3B). In addition, we conducted a qualitative analysis of the identified proteins. As shown in Fig. 3C, the ion scores of most of the identified proteins exceeded 20. As shown in Fig. 3D, we distributed the number of peptides for each identified protein, and almost 70% of them had two or more corresponding peptides. The above data indicated that the MS data in this study had a high degree of mass accuracy and could be further analyzed. The detailed information of the identified proteins is shown in Table S1.

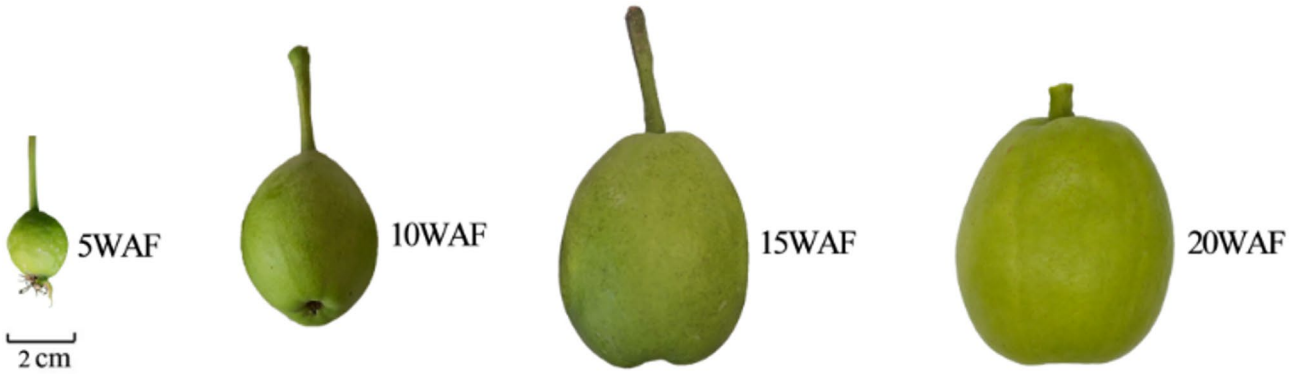

Fig. 1. Phenotypic traits of four Korla fragrant pear fruit development stages. They are 5 WAF, representing early development; 10 WAF and 15 WAF, representing middle development; and 20 WAF, representing ripening.

Name	Information
Database	UniProt-taxonomy_3766.fasta
Total Spectra	388901
Matched Peptide Spectra	102861
Peptides	50742
Unique peptides	36418
Identified proteins	8487
Quantifiable proteins	8246

Table 1. Summary of identified proteins.

Identification and analysis of differentially expressed proteins

A fold-change cutoff of ≥ 2.00 and $P < 0.05$ for proteins with upregulated expression and ≤ 0.50 and $P < 0.05$ for proteins with downregulated expression was applied to identify the DEPs between 10 and 5 WAF, 15 WAF and 5 WAF, and 15 WAF and 10 WAF. A total of 3762 DEPs were identified in the Korla fragrant pear at three fruit development stages (Table S1). Hierarchical cluster analysis revealed good reproducibility between different samples of the same group (Fig. 4A). A total of 1585 DEPs were identified at 10 WAF vs. 5 WAF, 896 of which presented upregulated expression and 689 of which presented downregulated expression (Fig. 4B, C). At 15 WAF vs. 5 WAF, 1373 DEPs presented upregulated expression, and 1523 DEPs presented downregulated expression (Fig. 4B, D), whereas at 15 WAF vs. 10 WAF, 1169 DEPs presented upregulated expression, and 1461 DEPs presented downregulated expression (Fig. 4B, E). In addition, Venn diagram analysis was performed to identify the common DEPs involved in Korla fragrant pear fruit development (Fig. 4F). Finally, 229 DEPs were differentially expressed (Fig. 4F) during pear fruit development. These 229 DEPs were subjected to in-depth analysis. In addition, 779 DEPs were differentially expressed between 10 WAF vs. 5 WAF and 15 WAF vs. 5 WAF, and 683 DEPs were differentially expressed between 10 WAF vs. 5 WAF and 15 WAF vs. 10 WAF, whereas 1574 DEPs were differentially expressed between 15 WAF vs. 5 WAF and 15 WAF vs. 10 WAF (Fig. 4F). These results indicate that more DEPs were expressed during ripening than during the early stage of pear fruit development.

GO enrichment analysis of the DEPs

GO enrichment analysis was performed for DEPs with up- and downregulated expression to determine the biological processes affected during fruit development in the Korla fragrant pear. In the GO enrichment analysis of the DEPs whose expression was upregulated in the 10WAF vs. 5WAF groups, 404 functional GO terms were significantly enriched, 156 of which were associated with biological processes (BPs), 179 with molecular functions (MFs), and 69 with cellular components (CCs) (Table S2). The results revealed several key biological processes, cellular components, and molecular functions, such as "translation," "protein folding," and "vacuolar transport" in the biological process category; "ribosome," "nucleosome," and "large ribosomal submit" in the cellular component category; and "structure constituent of ribosome," "RNA binding," "translation initiation factor activity" and "RNA binding," in the molecular function category, with functional upregulation of expression observed during pear fruit development from 5 to 10WAF (Fig. 5A, Table S2), suggesting that these components were more active during the early stage of fruit development and that many proteins were synthesized during that early stage of fruit development. GO enrichment analysis of DEPs with downregulated expression identified from the 10WAF vs. 5WAF groups revealed enrichment of 443 functional GO terms, 145 of which belonged to BPs, 79 to CCs, and 219 to MFs (Table S3). The top 30 enriched GO terms were obtained via Fisher's exact test (Fig. 5B). The results revealed "photosynthesis, light harvesting" and "protein-chromophore linkage" in the

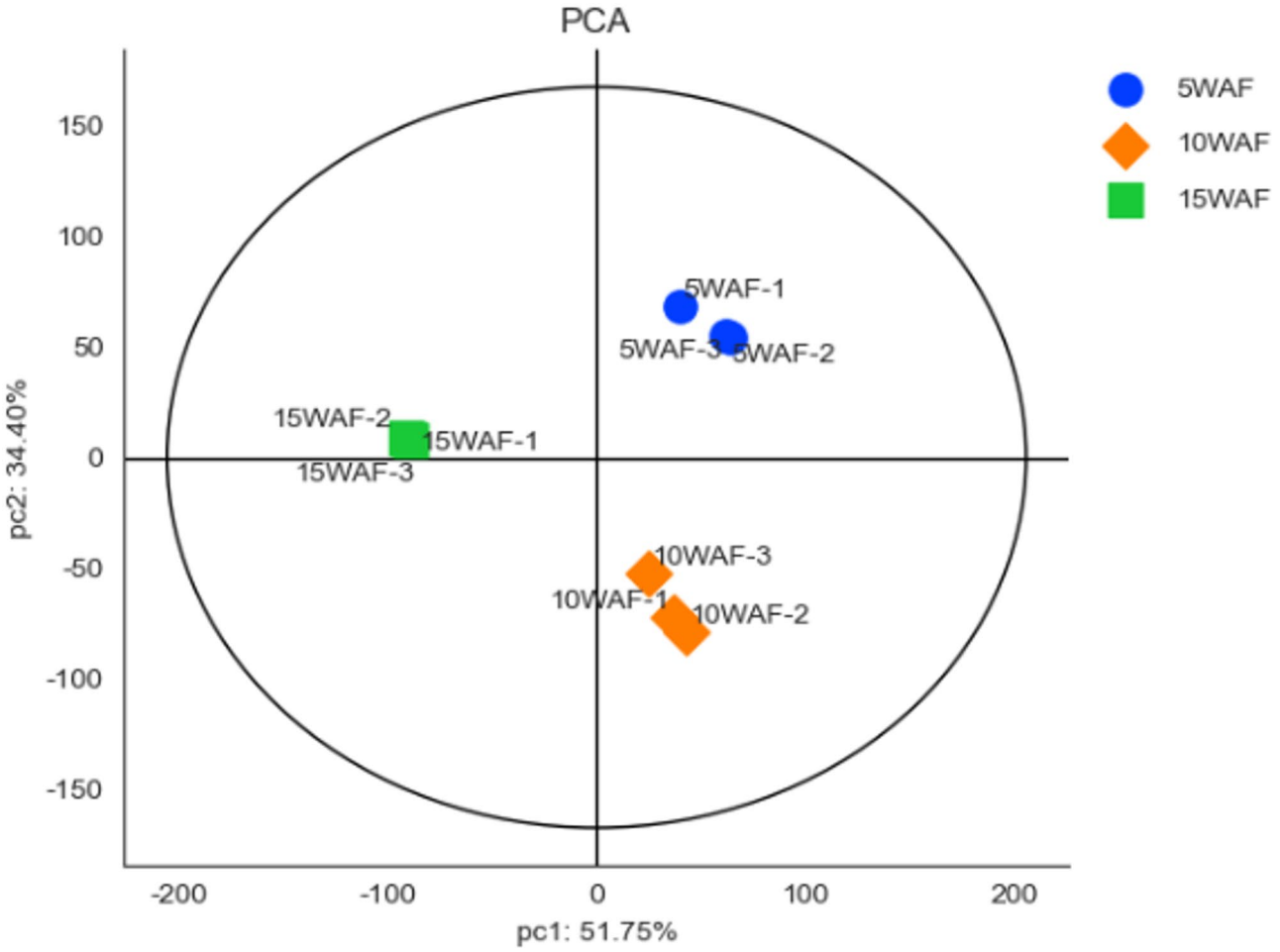

Fig. 2. PCA plots of proteins identified in Korla fragrant pear at three fruit development stages.

biological process category, "integral component of membrane," "Golgi membrane," and "mitochondrial inner membrane" in the cellular component category, and "transmembrane transporter activity" and "chlorophyll binding" in the molecular function category, indicating functional downregulation of expression for these categories during pear fruit development from 5 to 10WAF (Fig. 5B, Table S3).

In the GO enrichment analysis of the DEPs whose expression was upregulated in the 15WAF vs. 5WAF groups, the upregulated DEPs were significantly enriched in 834 functional GO terms, 303 of which belonged to BPs, 95 to CCs, and 436 to MFs (Table S4). The top 30 enriched GO terms were obtained (Fig. 5C), and the results revealed "intracellular protein transport," "vesicle-mediated transport," and "ubiquitin-dependent protein catabolic process" in the biological process category; "cytoplasm," "cytosol," and "exocyst" in the cellular component category; and "ATP binding," "metal ion binding," and "ATPase activity" in the molecular function category, with functional upregulation of expression observed during pear fruit development in the 15WAF group compared with the 5WAF group (Fig. 5C, Table S4). GO enrichment analysis of DEPs whose expression was downregulated in the 15WAF vs. 5WAF groups revealed enrichment of 674 functional GO terms, 249 of which were associated with BPs, 304 with MFs, and 121 to CCs (Table S5). The top 30 enriched GO terms were obtained (Fig. 5D), and the results revealed "carbohydrate metabolic process," "photosynthesis, light harvesting," and "protein-chromophore linkage" in the biological process category; "integral component of membrane," "chloroplast thylakoid membrane," and "mitochondrial inner membrane" in the cellular component category; and "chlorophyll binding," "threonine-type endopeptidase activity," and "superoxide dismutase activity" in the molecular function category, indicating functional upregulation of expression during pear fruit development in the 15WAF and 5WAF groups (Fig. 5D, Table S5).

GO enrichment analysis of the DEPs with upregulated expression identified from the 15WAF vs. 10WAF groups revealed enrichment of 784 functional GO terms, 271 of which were associated with BPs, 95 with CCs, and 418 with MFs (Table S6). The top 30 enriched GO terms were obtained (Fig. 5E), and the results revealed "intracellular protein transport," "vesicle-mediated transport" and "protein transport" in the biological process category; "cytoplasm," "membrane" and "endoplasmic reticulum membrane" in the cellular component category; and "ATP binding," "ATPase activity" and "small GTPase binding" in the molecular function category, indicating functional upregulation of expression during pear fruit development from the 10WAF to the 15WAF category (Fig. 5E, Table S6). GO enrichment analysis of DEPs with downregulated expression identified from

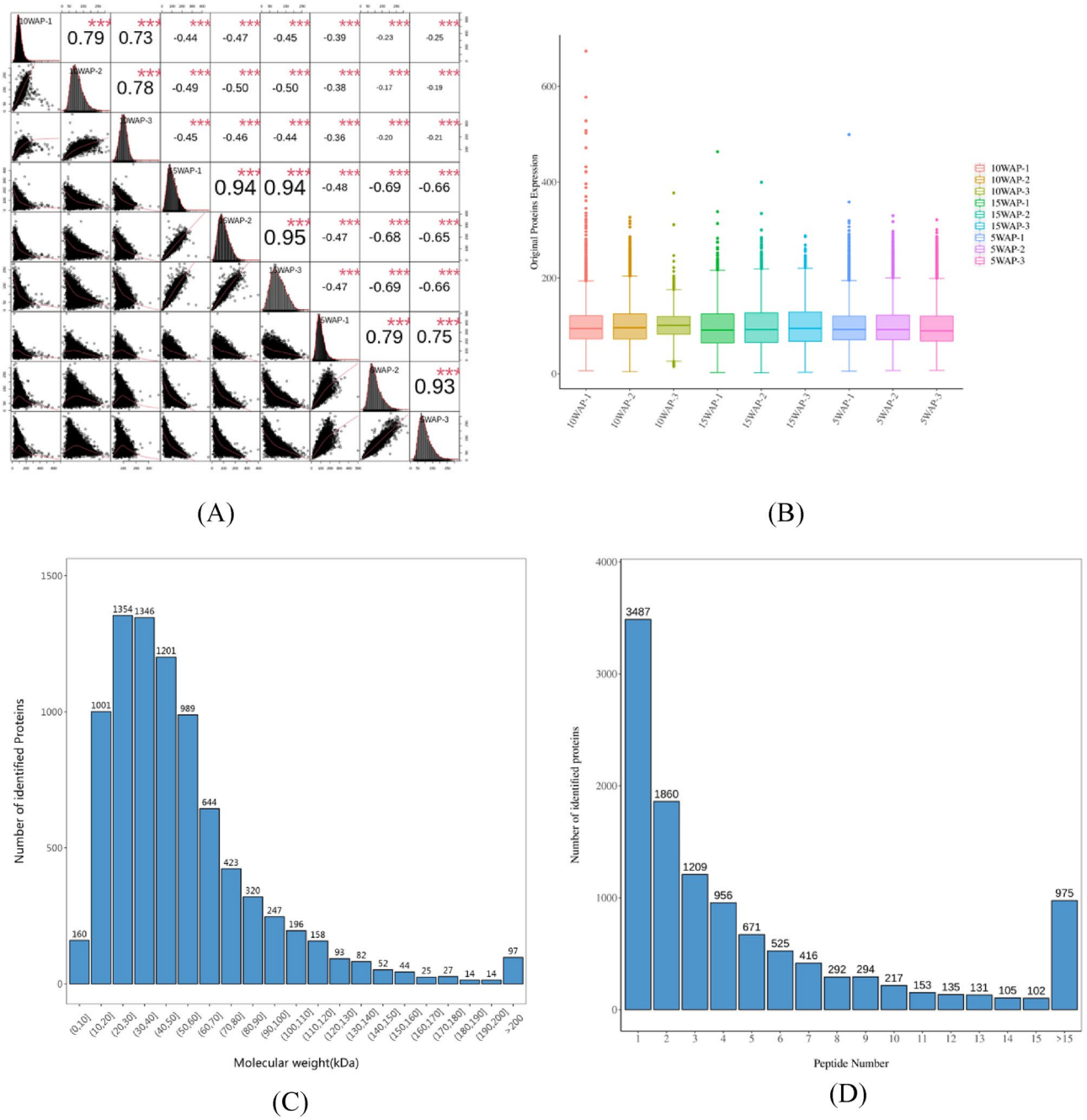

Fig. 3. **A** The upper triangle (above the diagonal) shows the correlation values between two samples, with asterisks indicating the level of significance (** $p < 0.05$, ** $p < 0.01$, and *** $p < 0.001$); the lower triangle (below the diagonal) presents the scatter plots of expression values for two samples, with the red curve representing the trend line, and the steeper the slope, the stronger the correlation between the two samples; the diagonal shows the distribution of expression levels for the samples themselves. B. The x-axis represents the sample names, and the y-axis represents the expression levels of the samples. A flatter box indicates a greater concentration of data, as does a shorter tail above the box. C. The molecular weight distribution of proteins is displayed based on the raw data, showing the number of proteins corresponding to different molecular weights. D. Number of peptide segments. In the raw data, each rectangle represents the distribution of identified proteins corresponding to different peptide counts.

the 15WAF vs. 10WAF groups revealed enrichment of 628 functional GO terms, 247 of which belonged to BPs, 115 to CCs, and 266 to MFs (Table S7). The top 30 enriched GO terms were obtained (Fig. 5F), and the results revealed "translation," "photosynthesis" and "photosynthesis, light harvesting" in the biological process category; "ribosome," "chloroplast thylakoid membrane" and "photosystem I" in the cellular component category; and "RNA binding," "structural constituent of ribosome" and "protein heterodimerization activity" in the molecular

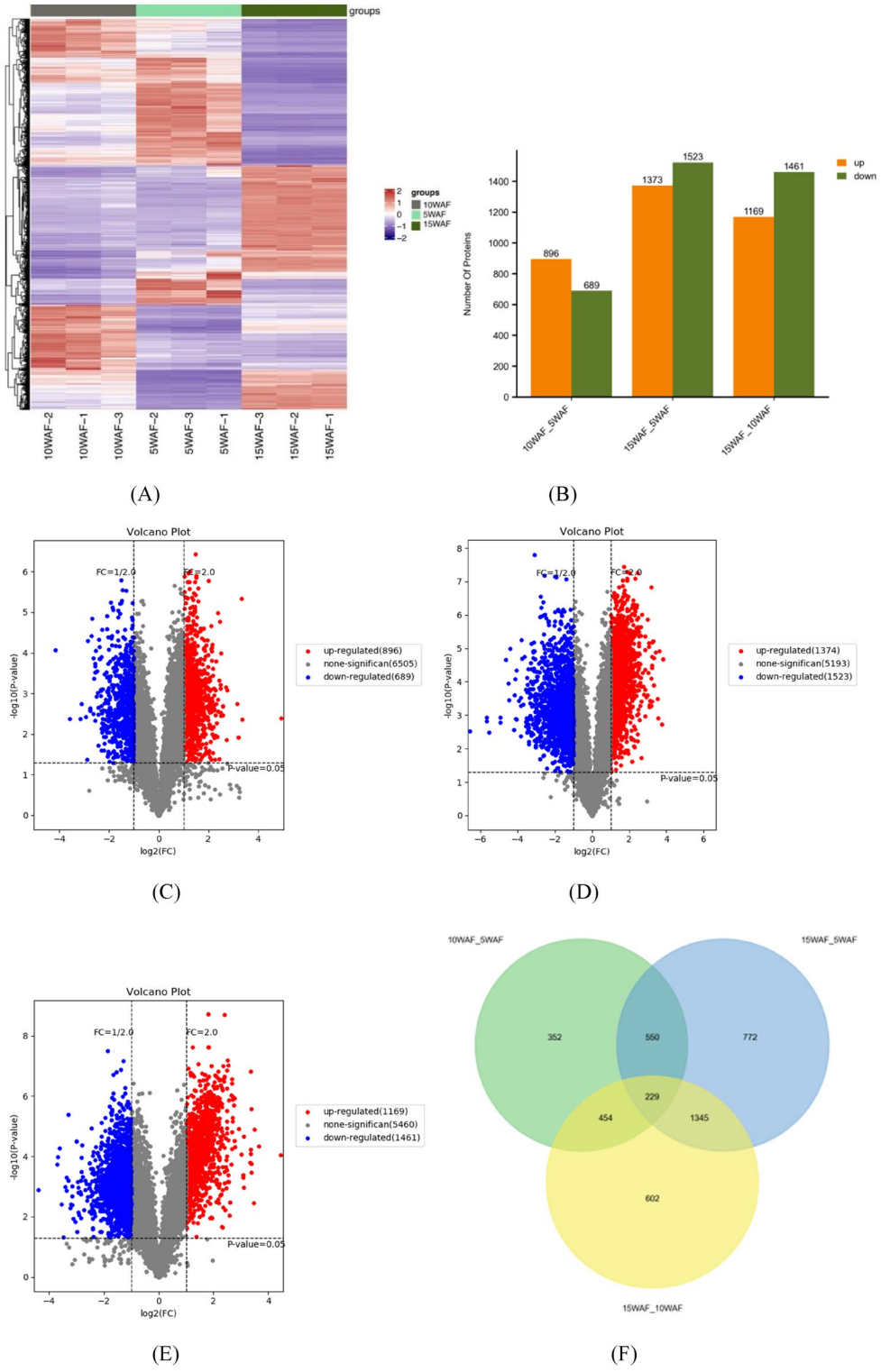

function category, indicating functional downregulation of expression during pear fruit development from 10 to 15WAF (Fig. 5F, Table S7).

KEGG pathway enrichment analysis of the DEPs

To obtain the most systematic and comprehensive understanding of the physiological and biochemical activation processes during fruit development, we used the KEGG pathway analysis method for pathway enrichment of DEPs. KEGG analysis was performed on DEPs from different comparator groups at three developmental stages. KEGG enrichment analysis of the DEPs from the 10 WAF vs. 5 WAF groups revealed enrichment of the top 20 pathways. Some of these enriched pathways were for ribosomes, oxidative phosphorylation, amino sugar and nucleotide sugar metabolism, flavonoid biosynthesis and phenylpropanoid biosynthesis (Fig. 6A). The significantly enriched KEGG pathways could be divided into four biological processes: (a) metabolite

◀**Fig. 4**. Numbers of DEPs in Korla fragrant pear fruits at three developmental stages. A, A clustering heat map of the three developmental stages of Korla pear fruit, indicating the differences and reproducibility among different developmental periods. B, The number of up- and downregulated differentially expressed proteins in three pairwise comparison groups, with the horizontal axis representing the comparison groups and the vertical axis representing the number of differentially expressed proteins. C, D, and E represent the volcano plots for 10 WAF vs. 5 WAF, 15 WAF vs. 5 WAF, and 15 WAF vs. 10 WAF, respectively. The horizontal axis is log2(FC), with values farther from 0 indicating greater differences, with the right side representing upregulation and the left side representing downregulation. The vertical axis is -log10(P value), with values farther from 0 indicating greater significance. Blue dots in the plot represent downregulated differentially expressed proteins, red dots represent upregulated differentially expressed proteins, and gray dots represent non-significant differentially expressed proteins. F, The Venn diagram analysis of differentially expressed proteins in the 10 WAF vs. 5 WAF, 15 WAF vs. 5 WAF, and 15 WAF vs. 10 WAF comparison groups.

synthesis, such as flavonoid biosynthesis, phenylpropanoid biosynthesis, and stilbenoid, diarylheptanoid and gingerol biosynthesis; (b) genetic information processing, such as ribosome, proteasome, and protein export; (c) photosynthesis, such as photosynthesis-antenna proteins; and (d) metabolism, amino sugar and nucleotide sugar metabolism, glycine, serine, and threonine metabolism, and phenylalanine metabolism.

A total of 111 pathways were enriched in the KEGG pathway enrichment analysis of the DEPs from the 15 WAF vs. 5 WAF groups (Table S8). The significantly enriched KEGG pathways could be divided into four categories: (a) cutin, suberin, wax, ubiquinone and other terpenoid-quinone biosynthesis; (b) metabolism, such as starch and sucrose metabolism; glycine, serine and threonine metabolism; (c) genetic information processing, such as aminoacyl-tRNA biosynthesis and protein processing in the endoplasmic reticulum; and d) photosynthesis, such as carbon fixation in photosynthetic organisms (Fig. 6B). In the KEGG pathway enrichment analysis of the DEPs between the 15WAF and 10WAF groups, a total of 114 pathways were enriched (Table S9), 13 of which were significantly enriched; these pathways were related primarily to ribosomes, the citrate cycle (TCA cycle), nucleocytoplasmic transport, fatty acid biosynthesis and photosynthesis (Fig. 6C).

Variations in soluble sugars during Korla fragrant pear fruit development

An ultra-performance liquid chromatography–electrospray tandem mass spectrometry (UPLC–ESI–MS) detection platform was used to determine the metabolite content changes in monosaccharides, disaccharides and trisaccharides during the four ripening stages (5WAF, 10WAF, 15WAF and 20WAF) of the Korla fragrant pear. First, PCA was performed on the sugar metabolic profiles of the Korla fragrant pear samples to assess the overall differences in sugar metabolism preliminarily among the four groups of samples and the extent of variation within each group as well as to determine the usability of the data. The PCA results demonstrated a trend in the separation of metabolomes between groups, indicating that there were differences in the metabolomes across the sample groups. The principal component scores revealed that PC1 and PC2 accounted for 56.68% and 19.33% of the variation among samples, respectively, with a total contribution rate of 76.01% (Fig. 7A). We detected a total of 27 soluble sugars, including 20 monosaccharides, 5 disaccharides and 1 trisaccharide, in Korla fragrant pear fruit (Fig. 7, Table S10). All 5 disaccharides, including cellobiose (Cel), lactose (Lac), maltose (Mal), trehalose (Tre) and sucrose (Suc), detected in this study were present at low concentrations during the early stages of fruit development but accumulated in large amounts from 15 to 20 WAF (Fig. 7), which may explain the greater sweetness of the Korla fragrant pear compared with other pear varieties. Moreover, the levels of seven monosaccharides, namely D-sorbitol, inositol, D-glucuronic acid, glucose, galactose, fructose (Fru), and 2-acetamido-2-deoxy-d-glucopyranose, rapidly increased from 10 to 20WAF (Fig. 7). However, the contents of the other 12 monosaccharides presented smooth variations across the first three stages but rapidly decreased to a lower content at the full ripening stage at 20 WAF, and the barium D-ribose-5-phosphate levels showed minute variations during fruit development (Fig. 7). With respect to trisaccharides, raffinose showed significantly high accumulation levels from 5 to 10 WAF and rapidly decreased to a low content at the full ripening stage.

Organic acid metabolism during Korla fragrant pear development

A PCA of the Korla fragrant pear samples, including quality control (QC) samples, was performed to gain a preliminary understanding of the overall differences in organic acid metabolism among the four groups and the magnitude of the variability between samples within groups. The PCA results revealed a trend toward metabolome separation between groups, suggesting differences in the metabolomes between sample groups. In the present study, three fruit developmental stages were used to analyze the repeatability of the samples that were subjected to the same treatments. The principal component scores revealed that PC1 and PC2 explained 51.15% and 16.51% of the variability among the samples, respectively, and the total contribution rate was 67.66% (Fig. 8A). The four fruit sample metabolomes were clearly separated and reproducible, and the replicates were compactly gathered, indicating the high reproducibility and scientific reliability of the data (Figs. 7A, 8A).

Multivariate statistics were performed to assess the differences among the organic acid profiles during the ripening stages. Hierarchical Cluster Analysis (HCA) was performed, and five main clusters were obtained according to the relative differences in organic acid accumulation patterns (Fig. 8B). We detected a total of 43 organic acids from Korla fragrant pear fruits in our study (Fig. 8B, Table S11). The organic acids involved in clusters 1 and 2 accumulated at high levels during the early stages of fruit development but rapidly decreased to a low level at the full ripening stage, at 20 WAF. The organic acids in cluster 3 were present at their highest levels 5 weeks after flower bloom. Moreover, the organic acid contents in cluster 3 decreased gradually from 10 to 20 weeks after flower blooming and were lowest at the full ripening stage at 20 WAF. However, the contents

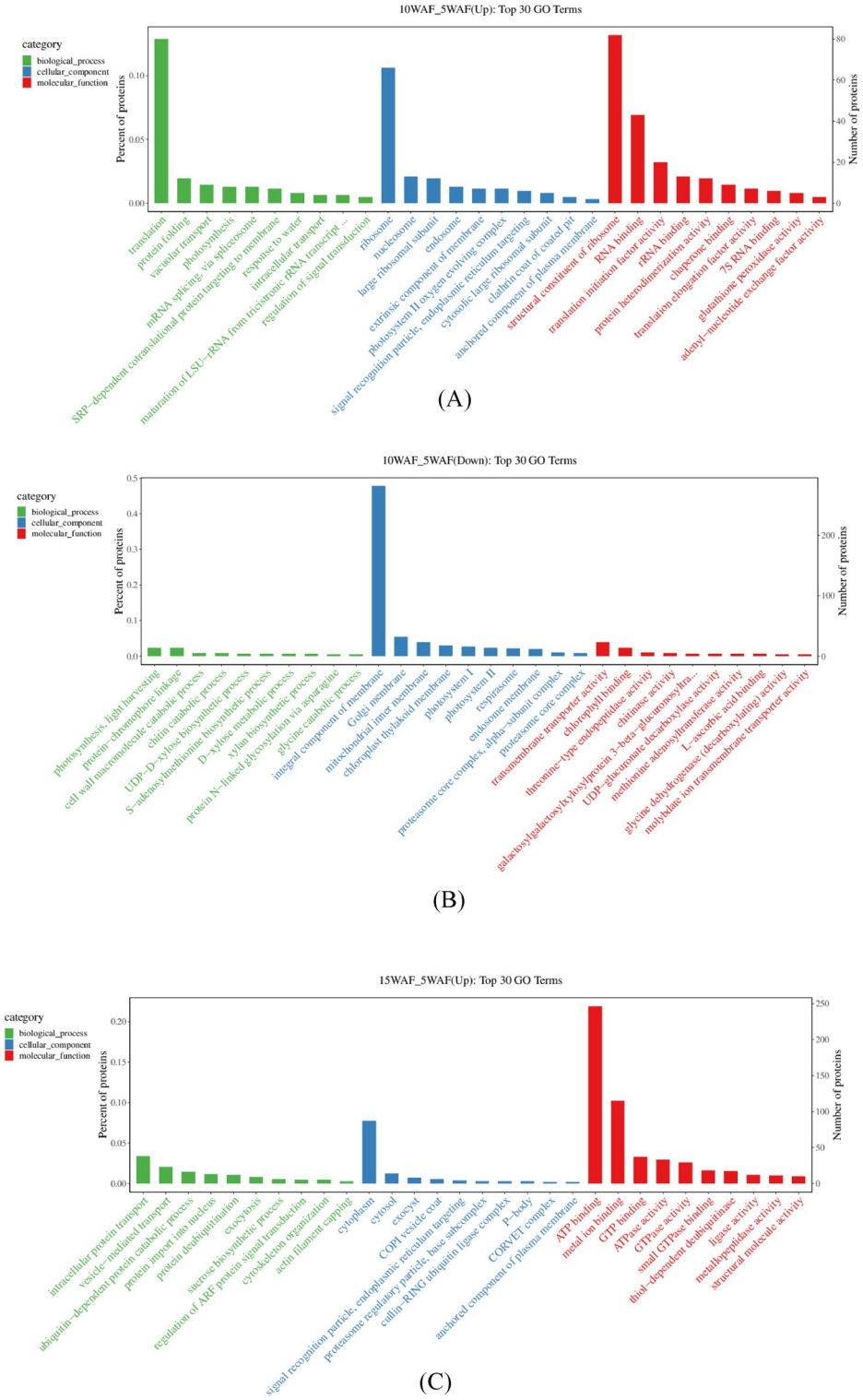

Fig. 5. Gene Ontology (GO) analysis of DEPs from different developmental stages of Korla fragrant pear fruits. (A) GO terms significantly enriched for upregulated expression in 10WAF vs. 5WAF; (B) GO terms significantly enriched for downregulated expression in 10WAF vs. 5WAF; (C) GO terms significantly enriched for upregulated expression in 15WAF vs. 5WAF; (D) GO terms significantly enriched for downregulated expression in 15WAF vs. 5WAF; (E) GO terms significantly enriched for upregulated expression in 15WAF vs. 10WAF; and (F) GO terms significantly enriched for downregulated expression in 15WAF vs. 10WAF.

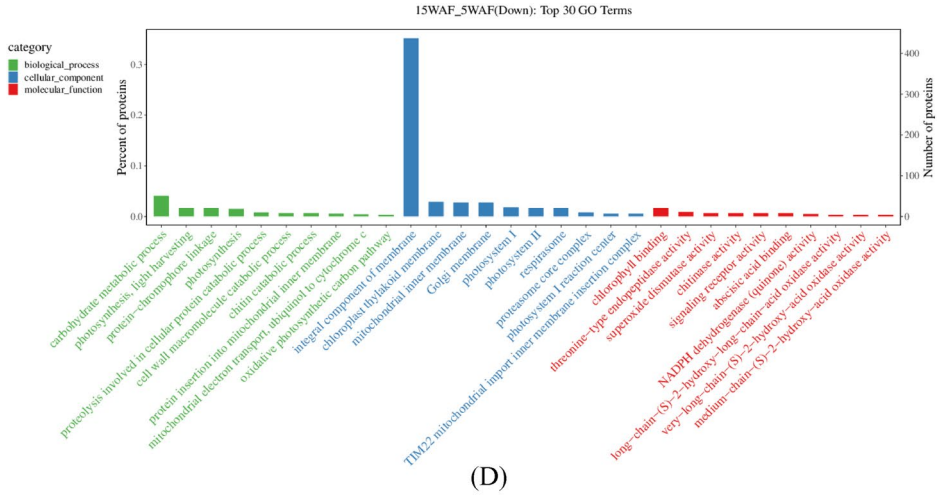

(D)

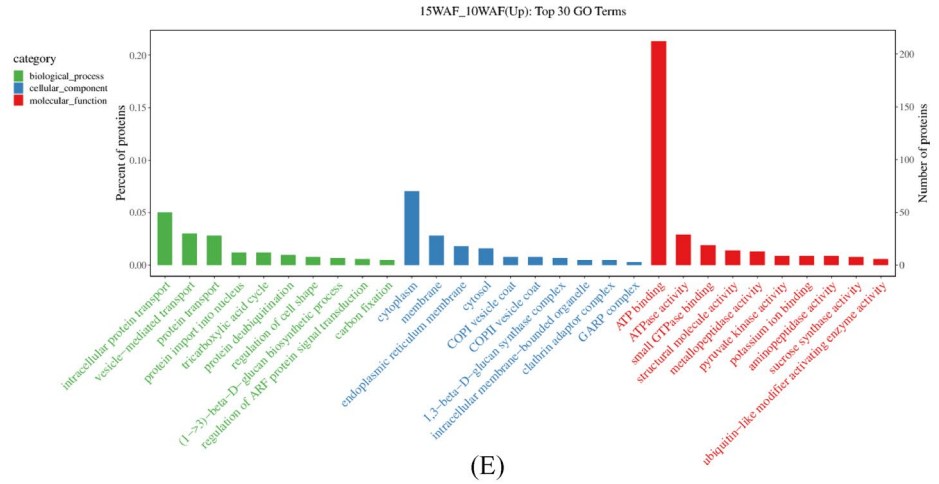

(E)

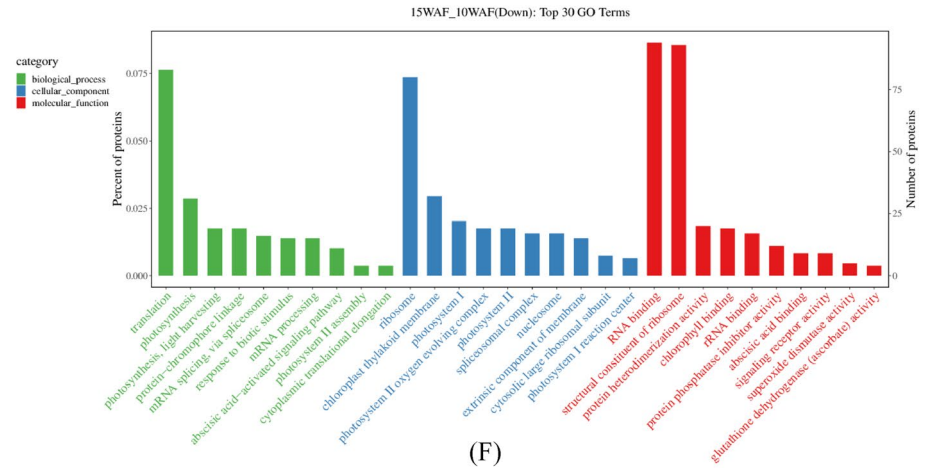

(F)

Fig. 5. (continued)

of the two organic acids in cluster 4 presented smooth variations among the four fruit developmental stages. Additionally, nine organic acids in cluster 5 gradually increased in content as the fruit developed and reached their highest contents at the full ripening stage (20WAF). Most of the organic acids are present at low levels in ripe Korla fragrant pears, and the ripe pear fruits used for consumption primarily contain the following nine organic acids: 2-hydroxyphenylacetic acid, homovanillic acid, pyruvic acid, cis-aconitic acid, 3-methyladipic acid, hydroxyphenyllactic acid, taurine, fumaric acid and tartaric acid.

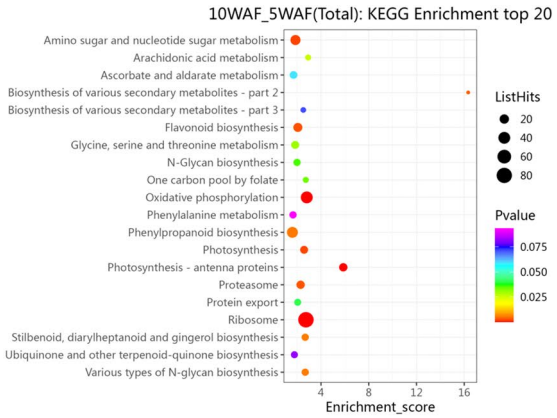

(A)

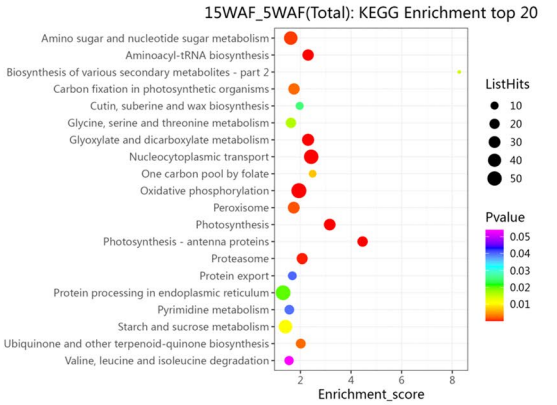

(B)

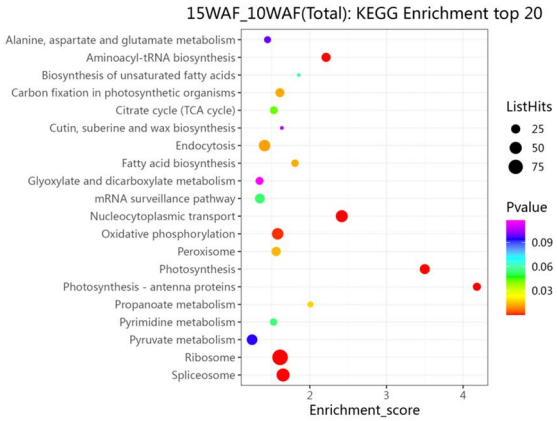

(C)

Fig. 6. KEGG pathway enrichment analysis of DEPs from different developmental stages of Korla fragrant pear fruits. The significantly enriched KEGG pathways in DEPs from (A) 10WAF vs. 5WAF, (B) 15WAF vs. 5WAF, and (C) 15WAF vs. 10WAF.

K-means clustering was used to classify all the differentially abundant organic acids further, into ten subclusters (Fig. 8C, Table S12). Subclusters 1, 7, 8 and 9 contained fifteen organic acids, whose contents gradually increased in pear fruits with the developmental stage. Subclusters 2, 3, 4, 6 and 10 contained 11 organic acids whose levels greatly increased at the first stage but then decreased at the full ripening stage. Interestingly, only the organic

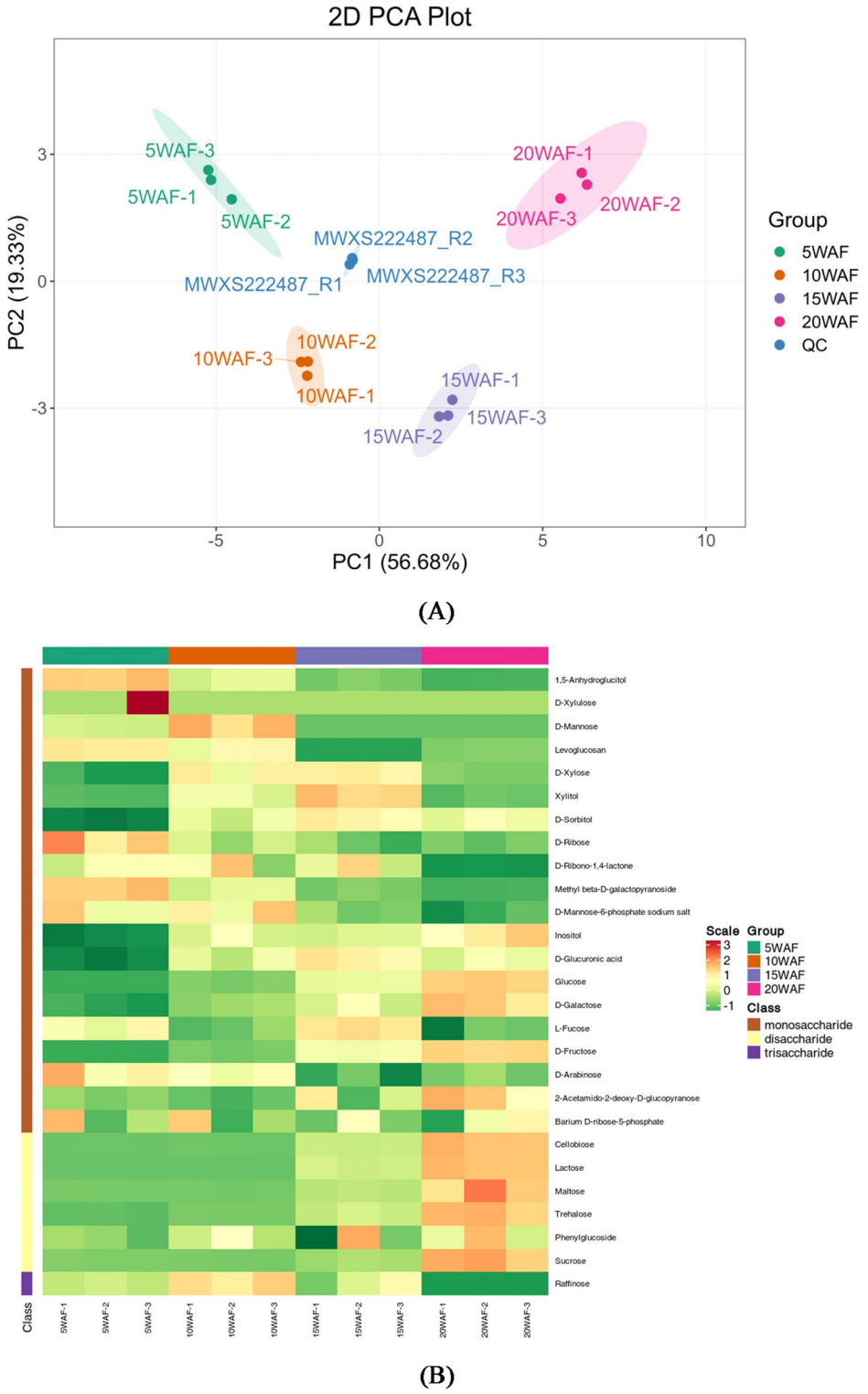

Fig. 7. Sugar metabolites detected by UPLC-ESI-MS during four fruit developmental stages. A: Score plots of principal components 1 and 2 represent high cohesion within groups and good separation among the four developmental stages. The sampling groups are color-coded as follows: green, 5WAF; orange-red, 10WAF; blue-purple, 15WAF; and pink-red, 20WAF B. The fold changes in the abundance of each metabolite among these four stages are displayed in a heat map in which the first stage (5WAF) was used as the calibrator. Three independent replicates were performed for each stage.

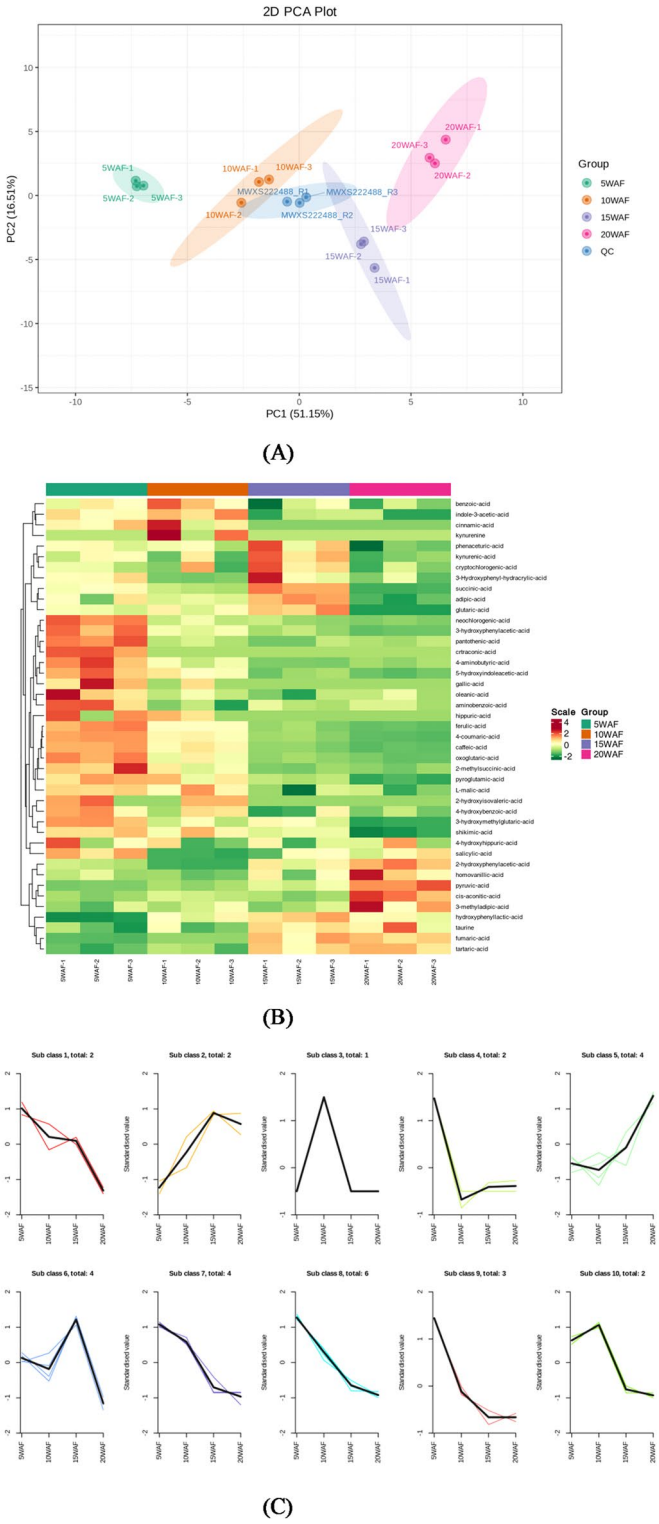

Fig. 8. Changes in abundances of organic acids (and their derivatives) during four fruit developmental stages. A: Score plots of principal components 1 and 2 represent high cohesion within groups and good separation among the four developmental stages. The sampling groups are color-coded as follows: green, 5WAF; orange–red, 10WAF; blue–purple, 15WAF; and pink–red, 20WAF. B: Heat map visualization. The profiles of all types of organic acids were normalized to complete the hierarchical clustering of their linkages. Each sample is represented by one column, and each organic acid is visualized in one row. Red indicates high abundance and green indicates relatively low metabolite abundance. C: K-means cluster analysis showing the dynamic accumulation of differentially abundant organic acid metabolites during the four fruit developmental stages.

acids in subcluster 5 gradually increased in content as the fruit matured and were highly accumulated in the ripe fruit.

Discussion

The fruits of the 'Korla' fragrant pear cultivar are rich in juice, with few stones, high sweetness, low organic acid content and a tantalizing aroma[32–34]. Fruit development and ripening are highly coordinated and irreversible biological processes that involve a series of changes in metabolic components, leading to the formation of mature edible fruit; proteins, as functional executors, are direct products of gene expression and directly influence biological processes[35,36]. However, the protein regulation and metabolic mechanisms involved in fruit and quality development in Korla fragrant pears are not clear. Given the importance of protein expression in regulating sugar and organic acid abundance changes, we compared the protein expression profiles of pears at 5, 10 and 15 weeks after flower blooming via TMT to identify proteins associated with quality changes in pear fruits. In addition, samples of pears at 5, 10, 15 and 20 weeks after flower blooming were used to detect the accumulation trends in sugars and organic acids. Proteomics labeling technology combined with a targeted metabolomic approach is a powerful method that has been successfully used to quantify and characterize changes in protein expression levels, such as in grapes[37,38], tomatoes[39], pecans[40], mangos[41], and other species[42,43]. In the present study, we are the first to use TMT-labeling technology combined with a targeted metabolomic approach to establish broad analyses on proteomics and associated metabolites to identify differentially expressed proteins and differentially abundant metabolites during pear fruit development.

Differentially expressed proteins associated with flavonoid biosynthesis in fruit development

Flavonoids constitute the second largest group of secondary metabolites in plants after alkaloids and play key roles in various biological events (growth and development, seed formation and germination, and photoprotection) and cellular processes (signaling and the scavenging of free radicals)[44,45]. Flavonoids are usually classified into six groups, namely, flavonols, flavonoids, dihydroflavonols, dihydroflavonoids, isoflavonoids and anthocyanins, and flavonoids with different structures contribute to pigment formation and phytohormone signaling in plants[44–46]. Proteins associated with flavonoid biosynthesis in this study were significantly differentially expressed between the 10WAF and 5WAF groups, with 1 protein (flavonol synthase/flavanone 3-hydroxylase) showing upregulated expression and 17 proteins (cinnamic acid 4-hydroxylase, caffeoyl-coenzyme A oxymethyltransferase, cytochrome P450, flavanone 3-hydroxylase, and anthocyanin reductase, among others) showing downregulated expression. Cinnamic acid 4-hydroxylase is the main enzyme in the phenylpropane pathway, is involved in the biosynthesis of secondary metabolites such as lignin and flavonoids and belongs to the cytochrome P450 family[46–49]. Caffeoyl coenzyme A oxymethyltransferase is a key enzyme in plant lignin synthesis and catalyzes the formation of feruloyl coenzyme A from caffeoyl coenzyme A. It also catalyzes the production of certain phenolic compounds, forming three classes of phenolic derivatives, such as flavonoids, lignans and anthocyanins[50,51]. Flavanone 3-hydroxylase (F3H) is a key enzyme that directs carbon flow to 3-hydroxylated flavonoid biosynthesis and is responsible for the biosynthesis of flavonols and anthocyanins[48,52]. Anthocyanins are essential for physiological and biochemical activities in plants, including antioxidant activity, protection against plant damage, stress responses, and the attraction of animals for pollination and seed dispersal[49,51].

The overexpression of LcF3H from *Lycium barbarum* in tobacco increased the flavan-3-ol content and improved tolerance to drought stress[52]. In addition, color variation in pear fruit depends on the content and proportion of chlorophyll, carotenoids, flavonoids and anthocyanins in the pericarp[53]. In this study, the significant downregulation of differentially expressed proteins such as cinnamic acid 4-hydroxylase, caffeoyl coenzyme A oxymethyltransferase, cytochrome P450, flavanone 3-hydroxylase, and anthocyanin reductase may have led to a decrease in the flavonoid content of balsam pears during the early development of Korla fragrant pears, which is similar to findings in strawberries, in which the downregulation of the expression of the key enzyme in flavonoids, F3H, led to a large decrease in anthocyanin content and a moderate decrease in flavonol content[54].

Differentially expressed proteins related to sugar metabolism and accumulation

The content and composition of soluble sugars are important indicators of pear fruit quality. To understand the molecular mechanism of sugar metabolism and accumulation in Korla fragrant pears, we identified the DEPs in pear fruits at three developmental stages. Based on the protein annotation, we retrieved all the proteins involved in sugar metabolism and accumulation.

Starch and sucrose metabolism

Several well-known enzymes related to the sucrose metabolism pathway have been reported to be determinants of sugar accumulation[55]. We identified 11 DEPs that were significantly upregulated at 10 WAF compared with those at 5 WAF or at 15 WAF compared with those at 10 WAF (Fig. 9), including sucrose synthase (A0A5N5I0S6, A0A5N5GEQ6, A0A5N5GDS4, and A0A5N5FQ57; EC:2.4.1.13), sucrose-phosphate synthase (A0A5N5H598; EC:2.4.1.14), and sucrose-6-phosphatase (A0A5N5FXX6; EC:3.1.3.24). Once sucrose is transported into pear fruit, it is reversibly catalyzed by sucrose synthase (SuSy), which enzymatically cleaves it to fructose and uridine diphosphate glucose (UDP-G) or adenosine diphosphate glucose (ADP-G)[56]. Many metabolic pathways, including energy production, primary metabolite production, and the synthesis of complex carbohydrates, require products produced by SuSy cleavage of sucrose as substrates for reactions[57]. The soluble sugar assay results revealed that the sucrose content was high in ripe pear fruit, further revealing the important role of these DEPs in regulating sugar accumulation in Korla fragrant pear fruit. Sucrose synthase is involved primarily in the synthesis of starch or cellulose and produces energy that is necessary for many compounds for fruit development[58].

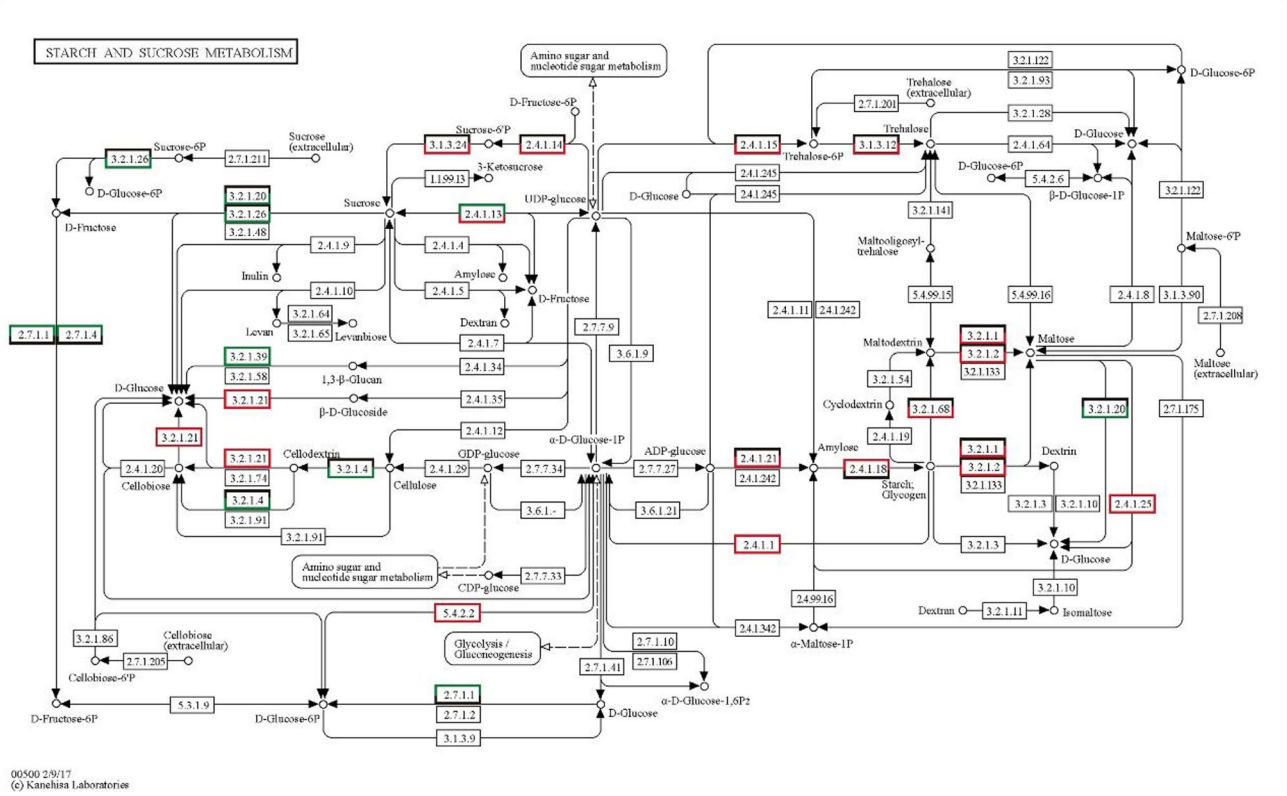

Fig. 9. Regulatory changes in the starch and sucrose metabolism pathways. Boxes indicate proteins, and circles indicate metabolites (sugars); boxes are red for upregulation, green for downregulation, and black for no significant difference; the top half of the box indicates the change in the 10 WAF vs. 5 WAF group, and the bottom half of the box indicates the change in the 15 WAF vs. 10 WAF.

Fructose and mannose metabolism

Sucrose is hydrolyzed into fructose and glucose by sucrose synthase or converting enzymes when it reaches the sink cells in the pear pulp, which helps to increase the content of fructose and glucose in the pulp[56,57]. In the fructose and mannose metabolism pathway, we identified 9 DEPs that were significantly differentially expressed at 10 WAF compared with 5 WAF or at 15 WAF compared with 10 WAF (Fig. 10), namely fructose-bisphosphate aldolase (A0A5N5FJB4, A0A5N5I6X5; EC: 4.1.2.13), beta-fructofuranosidase (B2NIA1; EC: 3.2.1.26), pyrophosphate–fructose 6-phosphate 1-phosphotransferase subunit alpha (A0A5N5I0I9; EC:2.7.1.90), ATP-dependent 6-phosphofructokinase (A0A5N5IJF4; EC:2.7.1.11) and sorbitol dehydrogenase-like isoform X1 (A0A5N5F4T3; EC: 1.1.1.14). Fructose diphosphate aldose and beta-fructofuranosidase act primarily to decompose fructose intermediates into other metabolites[59,60], and the expression of fructose diphosphate aldose and beta-fructofuranosidase decreased from 10 to 15 WAF, indicating that the decomposition of fructose intermediates decreased during the ripening period of Korla fragrant pear fruits and that more fructose accumulated in the fruits at the ripening stage. Additionally, four enzymes involved in mannose metabolism, including mannose-1-phosphate guanyltransferase alpha-like (A0A5N514S3; EC:2.7.7.13), mannan endo-1,4-beta-mannosidase (A0A5N5GYC0; EC:3.2.1.78), hexokinase (A0A5N5GTH7; EC:2.7.1.1), and GDP-mannose 4,6 dehydratase (A0A5N5GU29; EC:4.2.1.47), were significantly differentially expressed between 15 WAF vs. 10 WAF and 10 WAF vs. 5 WAF, respectively. The enzyme mannose-1-phosphate guanyltransferase alpha-like (A0A5N514S3; EC:2.7.7.13) was significantly upregulated in the comparison between 15 and 10 WAF, as it synthesizes GDP-mannose, which is the activated sugar nucleotide precursor for mannose residues in cell surface polysaccharides, thereby potentially reducing the content of mannose[61]. Additionally, as shown in Fig. 10, mannan endo-1,4-beta-mannosidase (A0A5N5GYC0; EC:3.2.1.78), an upstream enzyme involved in D-mannose synthesis, tended to decrease continuously from 5 to 15 WAF, thus inhibiting the synthesis of D-mannose. These results are consistent with our findings that fructose gradually accumulated and that the mannose content gradually decreased during the ripening period, as determined by UPLC-MS/MS (Fig. 7).

Galactose metabolism

The structure of galactose is similar to that of glucose, except for the location of one hydroxyl group[62]. Galactose is a monosaccharide, and our measurements of soluble sugar content revealed that galactose accumulates gradually as the fruit develops and matures, i.e., its content increases from 5 to 20 WAF (Fig. 7). Furthermore, in the galactose metabolism pathway, we identified 10 DEPs in the 10WAF group compared with the 5WAF group or in the 15WAF group compared with the 10WAF group (Fig. 11). Among these DEPs, only 3 presented

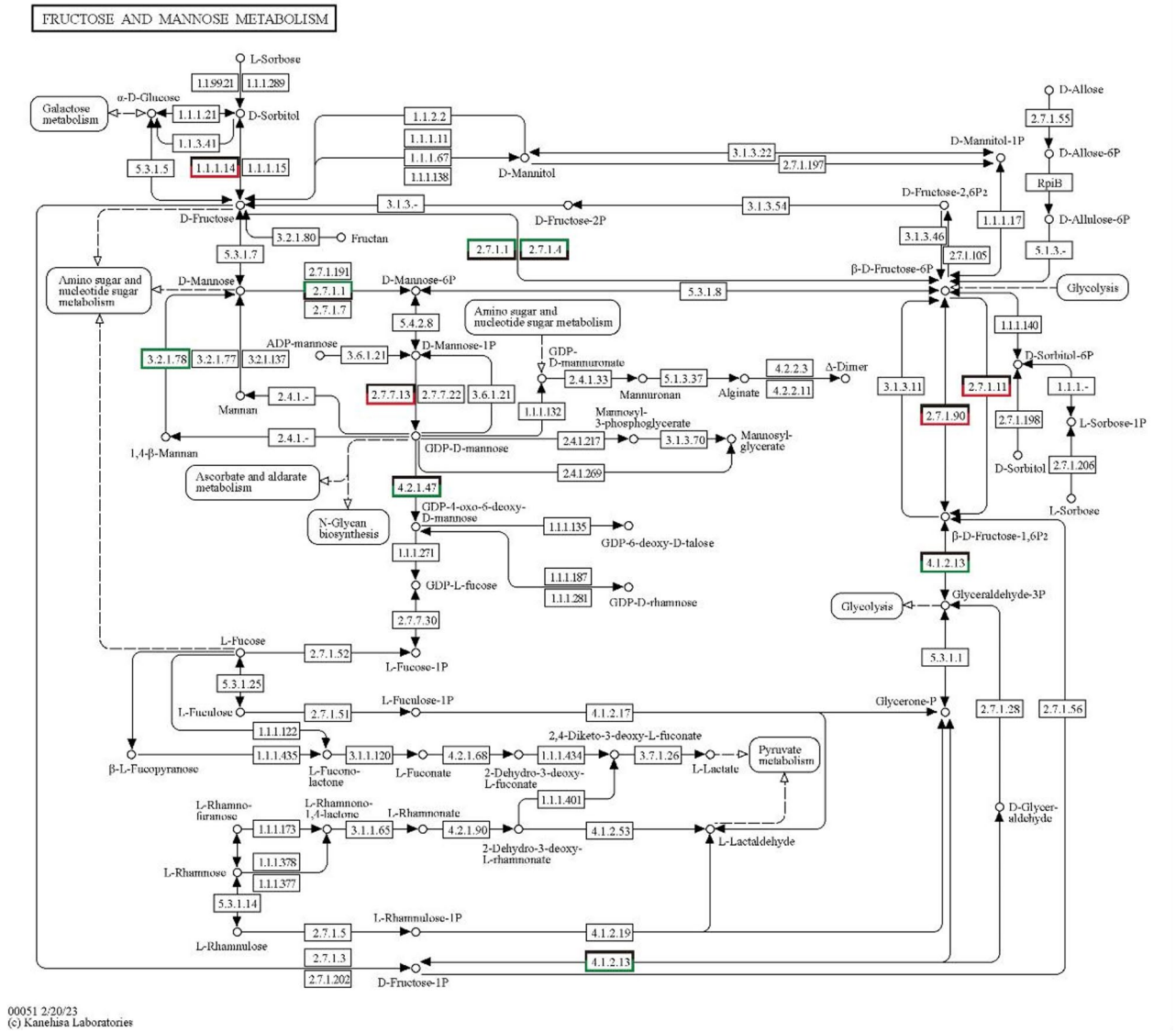

Fig. 10. Regulatory changes in the fructose and mannose metabolism pathways. Boxes indicate proteins, and circles indicate metabolites (sugars). The colors correspond with the pear proteins detected using TMT. Boxes are red for upregulation, green for downregulation, and black for no significant difference; the top half of the box indicates the DEPs at 10 WAF compared with those at 5 WAF and the bottom half of the box indicates the DEPs at 15 WAF compared with those at 10 WAF.

decreased expression, and all 8 DEPs were highly expressed; thus, these highly expressed proteins may promote galactose synthesis.

The soluble sugars in Korla fragrant pears are primarily fructose, glucose, sucrose and sorbitol[7,63,64]. Our results regarding soluble sugar determination via targeted metabolomics revealed five disaccharides in balsam pear fruit, namely Cel, Lac, Mal, Tre, and Suc. All the disaccharides detected in this study had low contents during the early stages of fruit development but accumulated in large amounts between 15 and 20 WAF, which may explain the higher sugar levels in the fruits of the Korla fragrant pear than in those of the other pear varieties. In addition, the levels of glucose, galactose and fructose rapidly increased from 10 to 20WAF during the ripening period, as determined by UPLC-MS/MS (Fig. 7). The sweetness and taste of different types of sugars differ: fructose is the sweetest, sucrose is the second sweetest, glucose is less sweet than fructose and sucrose, and the sweetness ratios of these three types of sugars are 1.75, 1.00 and 0.75, respectively[65–67]. The intensity of sweetness induced by maltose is generally approximately one-third of the molar value of sucrose[68,69]. High-sweetness soluble sugars accumulate in large quantities during ripening, providing strong evidence of the possible reasons for the greater sweetness of the Korla fragrant pear than the other pear varieties.

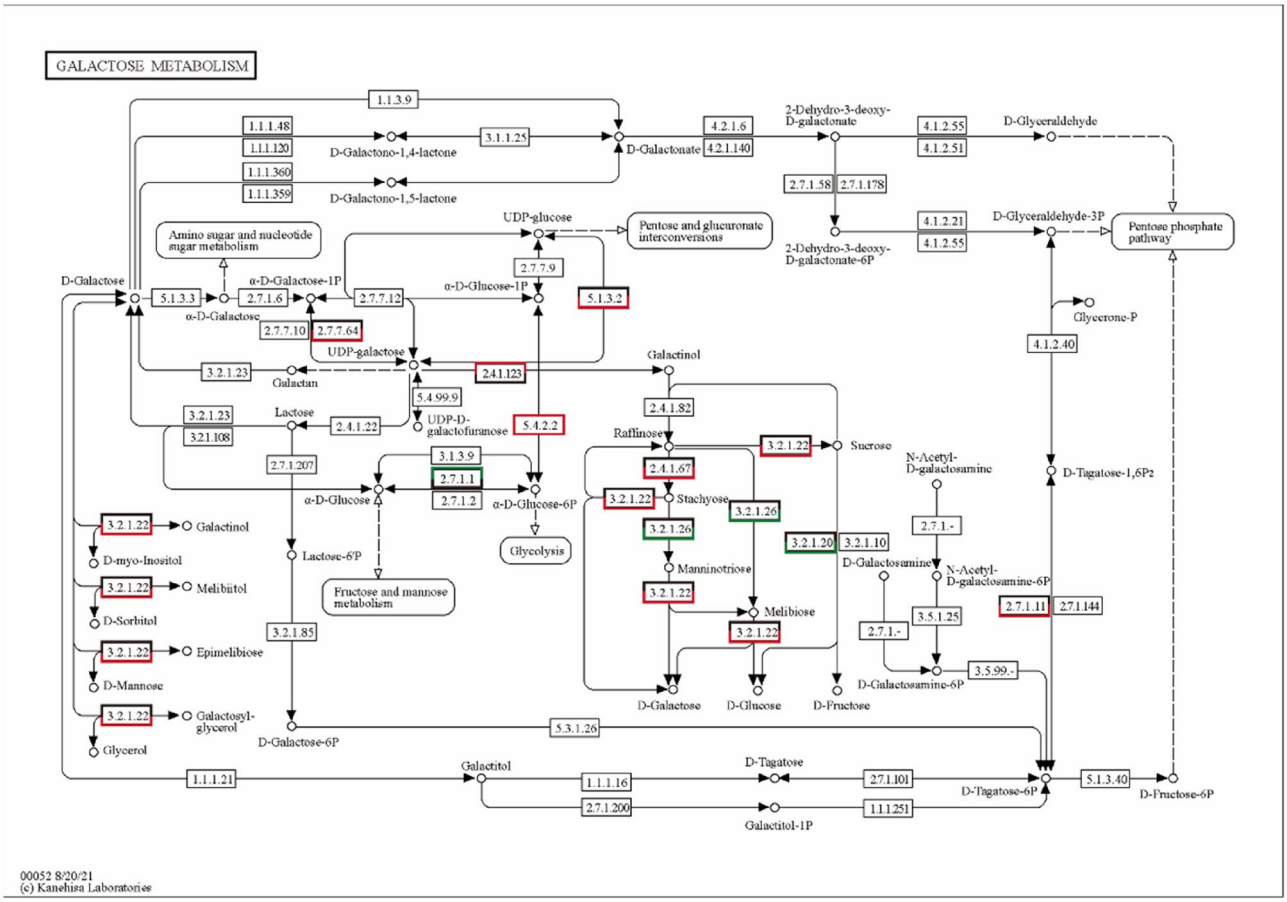

Fig. 11. Regulatory changes in the pathway of galactose metabolism. Boxes indicate proteins, and circles indicate metabolites (sugars). The colors correspond with the pear proteins detected using TMT. Boxes are red for upregulation, green for downregulation, and black for no significant difference; the top half of the box indicates the DEPs at 10 WAF compared with those at 5 WAF and the bottom half of the box indicates the DEPs at 15 WAF compared with those at 10 WAF.

Differentially expressed proteins related to organic acid metabolism

Organic acid metabolism is an important biological process that determines fruit flavor and palatability[70]. In this study, we identified several biological pathways related to organic acid metabolism and accumulation, such as the citrate cycle (TCA cycle), glycolysis/gluconeogenesis and phenylpropanoid biosynthesis. We identified 22 DEPs involved in the TCA cycle that were significantly changed in the 10WAF group compared with the 5WAF group or in the 15WAF group compared with the 10WAF group (Table 1). Among these, 12 DEPs were related to the metabolism of pyruvic acid (pyruvate), fumaric acid (fumarate), cis-aconitic acid (cis-aconitate), 2-oxoglutaric acid (oxoglutarate) and succinic acid (succinate) (Fig. 12). A multimer of dihydrolipoamide acetyltransferase forms the core of the pyruvate dehydrogenase multienzyme complex[68,71], and high expression of multiple dihydrosulfamide acetyltransferase subunits (A0A5N5I0E8, A0A5N5HFR7, A0A5N5I866; EC 2.3.1.12) was identified in this study. Pyruvate dehydrogenase, an important enzyme involved in the conversion of pyruvate to acetyl-CoA[72] (Fig. 12), was upregulated in both the 15 WAF vs. 10 WAF and the 10 WAF vs. 5 WAF comparisons in this study. A large amount of pyruvate is present in mature Korla fragrant pear fruits (20 WAF) (Fig. 8). However, before 20 WAF, there was no significant increase in pyruvate accumulation. Therefore, we speculated that from 5 to 15 WAF, pyruvate dehydrogenase was consistently upregulated, thereby promoting the conversion of pyruvate into acetyl-CoA. It is well known that glycolysis/gluconeogenesis plays a transitional role in sugar metabolism and organic acid metabolism, in which glycolysis is the process of breaking down glucose into two pyruvate molecules, and this process is the primary source of pyruvate generation. Figure 13 clearly shows that there are enzymes whose contents increase as D-glucose (glucose) is gradually broken down into pyruvate[73]. These include ATP-dependent 6-phosphofructokinase 6-like (A0A5N5IJF4; EC:2.7.1.11), pyrophosphate–fructose 6-phosphate 1-phosphotransferase subunit beta-like (A0A5N5I0I9; EC:2.7.1.90), NADP-dependent glyceraldehyde-3-phosphate dehydrogenase-like (A0A5N5GT63; EC:1.2.1.9), and pyruvate kinase 1 (A0A5N5I2V3, A0A5N5I6C8, A0A5N5HZY1, A0A5N5G528, A0A5N5HJ18, A0A5N5H3A8; EC:2.7.1.40). These enzymes tended to increase at 15 WAF compared with 10 WAF, whereas the changes were not significant at 10 WAF compared with 5 WAF, which is consistent with the trend in pyruvate changes during the ripening period. Therefore, we believe that these enzymes play a key role in promoting the synthesis of pyruvate. Overall,

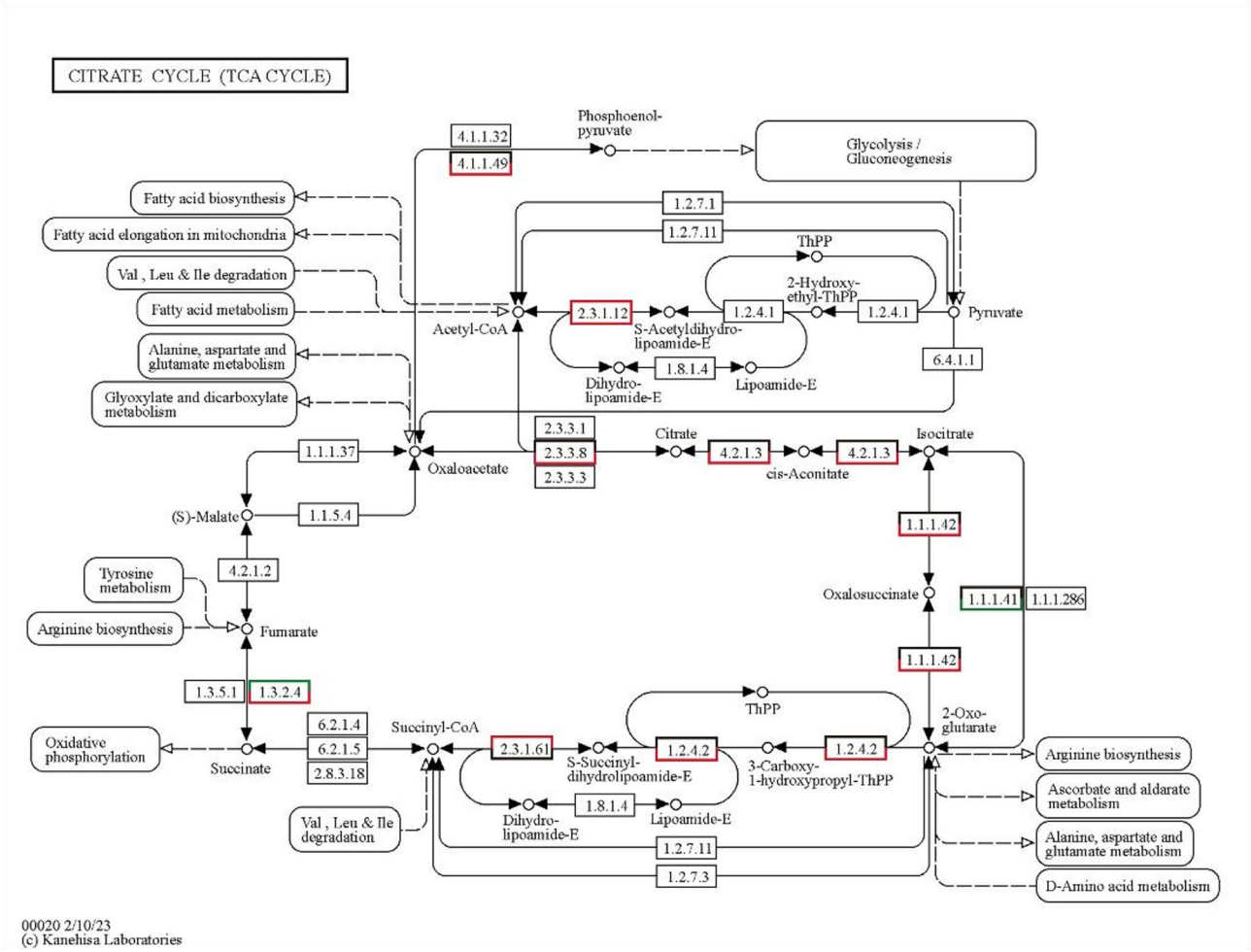

Fig. 12. Regulatory changes in the citrate cycle pathway. Boxes indicate proteins, and circles indicate metabolites. The colors correspond with the pear proteins detected using TMT. Boxes are red for upregulation, green for downregulation, and black for no significant difference; the top half of the box indicates the DEPs at 10 WAF compared with those at 5 WAF and the bottom half of the box indicates the DEPs at 15 WAF compared with those at 10 WAF.

through the process from D-glucose (glucose) to pyruvate and finally to acetyl-CoA, we preliminarily identified an activation mechanism of the TCA cycle. From 5 to 15 WAF, pyruvate was continuously converted into acetyl-CoA under high expression of dihydrosulfamide acetyltransferase subunits (A0A5N5I0E8, A0A5N5HFR7, A0A5N5I866; EC 2.3.1.12), which is why Fig. 7 shows that pyruvate was maintained at a low level except at 20 WAF. For the stage between 15 and 10 WAF, as the fruit continued to ripen, pyruvate began to accumulate and increase. Under the high expression of key glycolytic enzymes, the efficiency of glucose breakdown into pyruvate is increased. D-Glucose (glucose) also gradually increased in content during this process (Fig. 7), providing the necessary energy for the TCA cycle. This accumulation of pyruvate at the 15 WAF stage, which was continuously converted into acetyl-CoA, ultimately promoted the activation and initiation of the TCA cycle. Indeed, this activation process involves a complex regulatory mechanism involving multiple factors. The current data suggest a preliminary hypothesis for the activation mechanism of the TCA cycle in Korla fragrant pears, and these key enzymes will be the focus of subsequent research. The sixth step of the TCA cycle is catalyzed by succinate dehydrogenase (A0A5N5GVV6, EC 1.3.2.4) to produce fumaric acid[74,75]. We found that the expression of succinate dehydrogenase in Korla fragrant pear fruits first decreased but then increased during fruit development, whereas a large increase in fumaric acid abundance was detected at 15 WAF compared with 20 WAF (Figs. 7, 12). However, the high accumulation of fumaric acid and the fact that fumaric acid synthesis is catalyzed by succinic acid led to a significant reduction in the content of succinic acid during the ripening of the Korla fragrant pear. Furthermore, the levels of aconitate hydratase (A0A5N5GEQ9, E.C. 4.2.1.3) and isocitrate dehydrogenase (A0A5N5G492, A0A5N5G920; EC 1.1.1.42) in the TCA cycle increased substantially later in fruit development (Fig. 12). Aconitate hydratase interconverts citrate and cis-aconitate, and citrate can be isomerized to isocitrate via cis-aconitate catalysis by aconitrate hydrolase[76,77]. Isocitrate dehydrogenase is a key enzyme in the TCA cycle, and the reaction catalyzed by isocitrate dehydrogenase provides an alternative pathway for the production of 2-oxoglutarate[78,79]. Thus, the high expression of aconitate hydrolase and isocitrate

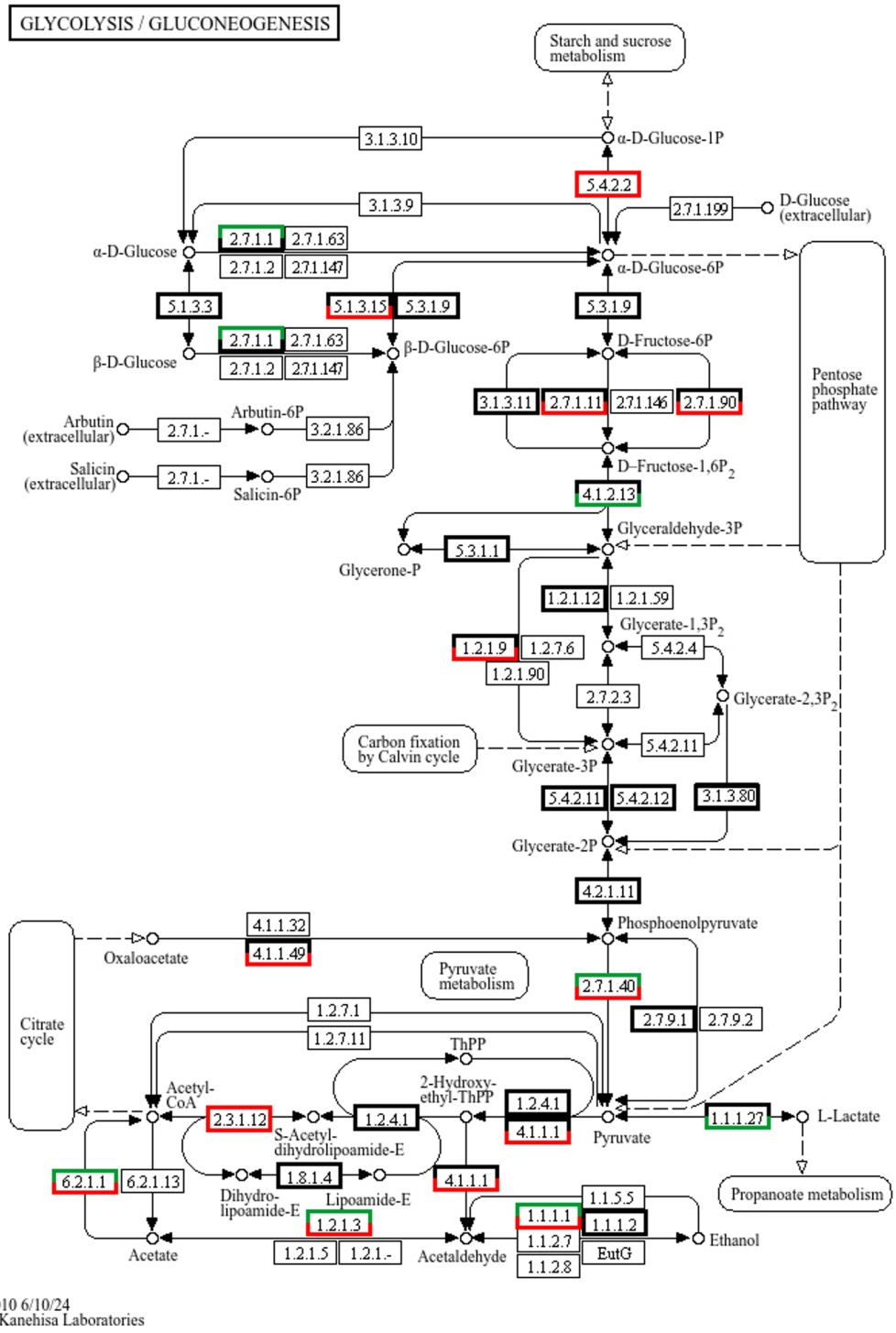

Fig. 13. Regulatory changes in the glycolysis/gluconeogenesis pathway. Boxes indicate proteins, and circles indicate metabolites. The colors correspond with the pear proteins detected using TMT. Boxes are red for upregulation, green for downregulation, and black for no significant difference; the top half of the box indicates the DEPs at 10 WAF compared with those at 5 WAF and the bottom half of the box indicates the DEPs at 15 WAF compared with those at 10 WAF.

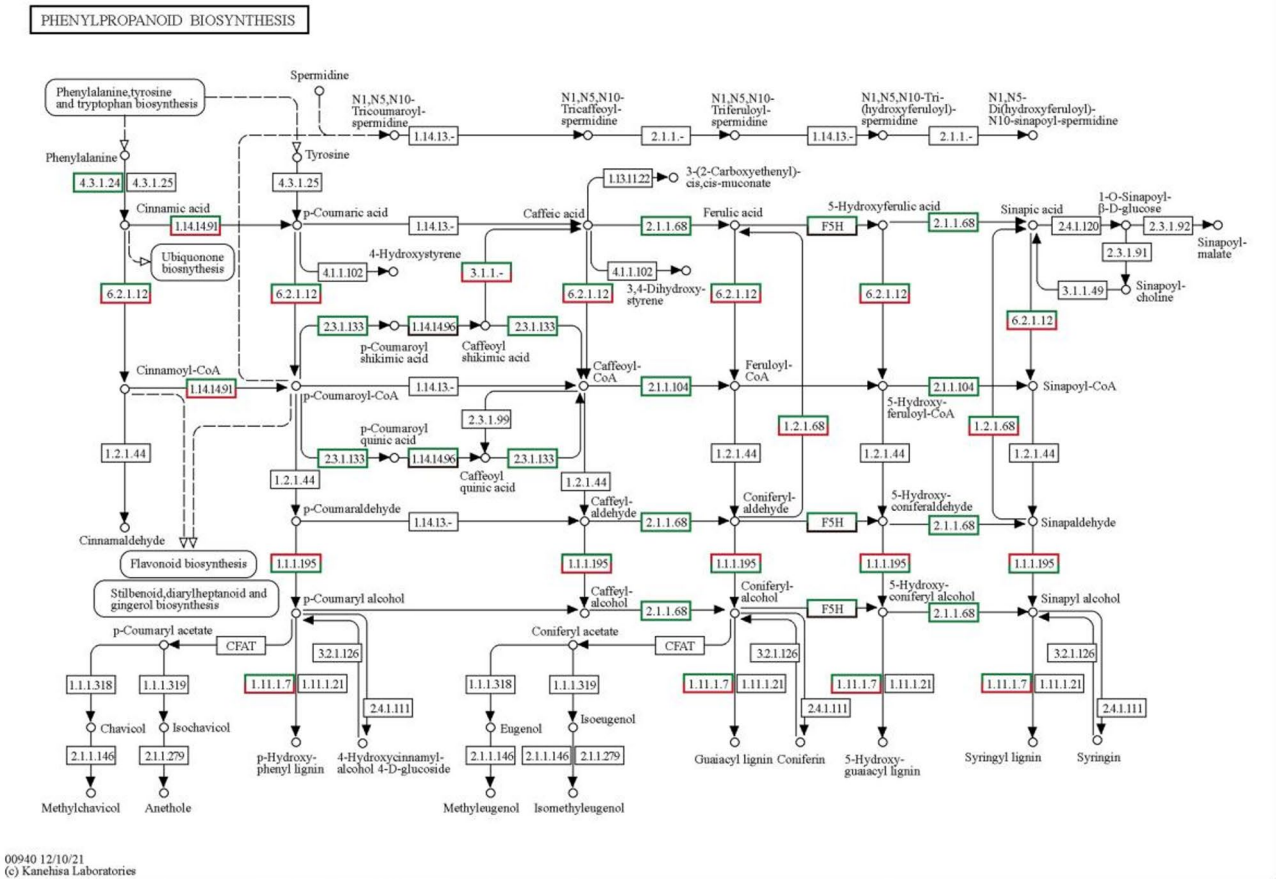

Fig. 14. Regulatory changes in the phenylpropanoid biosynthesis pathway. Boxes indicate proteins, and circles indicate metabolites. The colors correspond with the pear proteins detected using TMT. Boxes are red for upregulation, green for downregulation, and black for no significant difference; the top half of the box indicates the DEPs at 10 WAF compared with those at 5 WAF and the bottom half of the box indicates the DEPs at 15 WAF compared with those at 10 WAF.

dehydrogenase may have facilitated the accumulation of cis-aconitate and 2-oxoglutarate. In this study, we detected a large accumulation of fumaric acid, pyruvic acid, cis-aconitic acid and 2-oxoglutaric acid in the TCA cycle and a substantial decrease in the succinic acid content, suggesting that the differentially expressed protein results were highly concordant with the results of the organic acid measurements (Fig. 8B).

In addition, several key enzymes related to "phenylpropanoid biosynthesis" were identified during Korla fragrant pear fruit development, including caffeoylshikimate esterase-like (A0A5N5F542, E.C. 3.1.1-), phenylalanine ammonia-lyase (A0A5N5F468, E.C. 4.3.1.24), 4-coumarate-CoA ligase-like 7 (A0A5N5FZ22, E.C. 6.2.1.12), cinnamate 4-hydroxylase 3 (A0A385EIG2, E.C. 1.14.14.91), caffeic acid 3-O-methyltransferase (A0A5N5F701, A0A5N5FCH1; E.C. 2.1.68) and ferulate 5-hydroxylase (A0A3T0TV10) (Fig. 14). Cinnamic acid, a ubiquitous alpha beta unsaturated acid, can be hydrogenated by cinnamate 4-hydroxylase 3 to produce p-coumaric acid or catalyzed by 4-coumarate-CoA ligase-like 7 to produce cinnamoyl-CoA[80]. Thus, the high expression of cinnamate 4-hydroxylase 3 and 4-coumarate-CoA ligase-like 7 from 10 to 15WAF may have facilitated the production of p-coumaric acid and cinnamoyl-CoA from cinnamic acid, which in turn led to a decrease in cinnamic acid content. We detected a substantial decrease in the cinnamic acid content from 10 to 20 weeks after flower blooming, and the cinnamic acid content was lowest at the full ripening stage at 20 WAF, suggesting that the DEP results were highly concordant with the cinnamic acid measurement results (Fig. 8B).

Materials and methods

Plant materials and sampling

The pear variety used in this study was the Korla fragrant pear (2n = 34), whose variety name is 'Korla fragrant pear', which is an ancient local variety in southern Xinjiang and is most cultivated and well known in the Korla region[81]. This experiment was conducted at the Korla fragrant pear experimental site at the Xinjiang Academy of Agricultural Reclamation in April 2021. Korla fragrant pear fruit samples collected at three stages of fruit development were obtained from the pear depository at the Xinjiang Academy of Agricultural Reclamation experimental sites. Samples were taken at four time points depending on the 2021 pear development status:

5 weeks after flower blooming (WAF) represents the early pear fruit development stage; 10 WAF represents the middle pear fruit development stage; 15 WAF represents the near-ripening pear fruit stage; and 20 WAF represents the fully mature pear fruit stage. The phenotypic traits of the pear fruits are shown in Fig. 1. Approximately 10–20 pear fruits, depending on the fruit size at different stages, were collected from four different trees. Five WAF, 10 WAF and 15 WAF samples were used for proteomic analysis, and 5 WAF, 10 WAF, 15 WAF and 20 WAF samples were used for metabolite (organic acids and sugars) analysis. Three biological replicates were used at each developmental stage. Finally, fruit samples from the same stage were mixed after washing and kernel removal, cut into slices, snap-frozen in liquid nitrogen and transported directly back to the laboratory. All collected samples were stored at − 80 °C until use for proteomic and metabolite (organic acids and sugars) analyses.

Protein extraction and trypsin digestion

P. sinkiangensis Yü fruit samples were ground to a fine powder in liquid nitrogen. Protein was extracted via 4% (w/v) SDS in 100 mM Tris HCl (pH 7.6, 0.1 M DTT). Two hundred micrograms of protein was taken from each sample and digested using a filter-aided proteome preparation (FASP) method for trypsin digestion.

The total proteins from pear fruits at three different developmental stages (5 WAF, 10 WAF, and 15 WAF) were extracted. Protein extraction was performed according to a previously described protocol[76]. Finally, Bradford protein quantification were used to accurately quantify protein concentrations, and bovine serum albumin was used as the standard.

Protein TMT labeling, HPLC fractionation, and LC–MS/MS analysis

One hundred micrograms of trypsin-digested protein was taken from each sample and labeled with TMT (Thermo Fisher Scientific, Rockford, IL, USA) according to the manufacturer's instructions. Three 5 WAF samples were labeled with 126-tag, 127 N-tag, 127C-tag; 10 WAF samples were labeled with 128 N-tag, 128 C-tag, and 129 N-tag; and the 15 WAF samples labeled with 129 C-tag, 130 N-tag, and 130 C-tag, respectively. The labeled samples were mixed in equal amounts in new microcentrifuge tubes. Peptides from each group were pooled together and graded with a high-pH reversed-phase peptide fractionation kit. Each converted peptide sample was vacuum-dried, lyophilized, and then solubilized in 12 µL of 0.1% formic acid to increase the sensitivity and accuracy of the assay. The peptide concentrations were determined with a spectrometer at OD280.

Next, each fractionated sample was separated using an HPLC system with an easy nLC with a nanoliter flow rate using buffer A (0.1% formic acid aqueous solution) and buffer B (0.1% formic acid in 84% acetonitrile aqueous solution). The chromatographic column was equilibrated with 95% buffer A. The samples were loaded into the loading column via an autosampler (Thermo Scientific Acclaim PepMap100, 100 µm × 2 cm, nano Viper C18) and passed through an analytical column (Thermo Scientific EASY column, 10 cm, ID75 µm, 3 µm, C18-A2) for separation at a flow rate of 300 nL/min. These samples were analyzed on a Q Exactive mass spectrometer. The positive ion detection method was used, and the scan range for the precursor ions was 300–1800 m/z. The resolution of the primary mass spectrometer was 70,000 at 200 m/z, the automatic gain control (AGC) target was 1e6, the maximum IT was 50 ms, and the dynamic exclusion time was 60.0 s. To determine the m/z ratio of the peptides and peptide fragments, 20 fragmentation maps were collected after each scan. The MS2 activation type was HCD, and the isolation window was 2 m/z. The resolution of the secondary mass spectrum was 17,500 at 200 m/z (TMT 6-plex) or 35,000 at 200 m/z (TMT 10-plex), with a 30 eV normalized collision energy and 0.1% underfill. All the above procedures were performed by Shanghai Applied Protein Technology Co. Ltd. The mass spectrometry proteomics data have been deposited in the ProteomeXchange Consortium with the dataset identifier.

Protein identification and quantification

The raw files were processed using Mascot version 2.2 and Proteome Discoverer version 1.4 with the standard settings against a *Pyrus bretschneideri* protein database (uniprot_ *P. bretschneideri*_ 3766.fasta, downloaded 2021/11/12). Trypsin was selected as a random cleavage enzyme, and the parameter of maximum missed cleavages was set to 2. The peptide mass tolerance was set to ± 20 ppm, and the fragment mass tolerance was 0.1 Da. The database schema was used as a decoy to calculate the FDR. The screening criterion for credible peptides was an FDR ≤ 0.01. The protein ratios were calculated from the median of unique peptides only. All the peptide ratios were then normalized to the median protein ratio. The median protein ratio was 1 after protein normalization. Plant-mPLoc software was used to predict the subcellular location of the identified proteins.

Sugars and organic acid metabolite profiling

The preparation of fruit pulp samples, extract analysis, and the qualitative and quantitative determination of sugar and organic acid metabolites were optimized according to the methods previously described by Umer et al.[82], with the following steps. Approximately 200 mg of each sample was accurately weighed and placed in a 2 mL Eppendorf tube. Then, 0.6 mL of 2-chlorophenylalanine (4 ppm) methanol (− 20 °C) was added, and the mixture was vortexed for 30 s; 100 mg of glass beads was added, and the samples were placed into a TissueLysis II tissue grinding machine. The samples were ground at 25 Hz for 60 s. The tubes were placed in an ultrasonic bath at room temperature for 15 min and then centrifuged at 25 °C for 10 min at 1750 × g, after which the supernatant was filtered through a 0.22 µm membrane to obtain the prepared samples for liquid chromatography–mass spectrometry (LC–MS); 20 µL of each sample was mixed and used as a quality control (QC) sample (these QC samples were used to monitor deviations of the analytical results from these pooled mixtures and compare them to the errors caused by the analytical instrument itself). The remaining extracts were used for LC–MS detection.

Chromatographic separation was performed using a QTRAP® 6500 + system equipped with an ACQUITY UPLC® HSS T3 (150 × 2.1 mm, 1.8 µm, Waters) column maintained at 40 °C. The temperature of the autosampler

was 8 °C. The gradient elution of analytes was performed using 0.1% formic acid in water (D) and 0.1% formic acid in acetonitrile (C) or 5 mM ammonium formate in water (B) and acetonitrile (A) at a flow rate of 0.25 mL/min. Two microliters of each sample was injected after equilibration. An increasing linear gradient of solvent A (v/v) was used as follows: 0–1 min, 2% A/C; 1–9 min, 2–50% A/C; 9–12 min, 50–98% A/C; 12–13.5 min, 98% A/C; 13.5–14 min, 98–2% A/C; and 14–20 min, 2% C-positive model (14–17 min, 2% A-negative model). The samples were separated by chromatography and then subjected to mass spectrometry analysis. The mass spectrometry conditions were as follows: the temperature was 550 °C, the mass spectrometry voltage in positive ion mode was 5500 V, the mass spectrometry voltage in negative ion mode was -4500 V, and the curtain gas (CUR) pressure was 35 psi. In the Q-Trap 6500 + , each ion pair was subsequently scanned and detected based on the optimized declustering potential (DP) and collision energy (CE).

We conducted qualitative analysis of the mass spectrometry data via the Metware Database (MWDB) constructed with standard compounds. For the quantification of metabolites, we employed the multiple reaction monitoring (MRM) method to complete the quantification process, and we referred to and optimized the specific operational procedures from the studies by Wang et al.[83] and Xu et al.[84]. Specifically, after the mass spectrometry data were obtained, analyst 1.6.3 software was used to integrate the chromatographic peaks of all the target substances. We then established standard curves (Table S13, S14), with the standard concentrations for the metabolites as follows: for sugar metabolites, the concentrations were 0.001, 0.005, 0.01, 0.05, 0.1, 0.5, 1, 2, 5, 10, 15, 20, 25 and 50 μg/mL; and for organic acid metabolites, the concentrations were 0.01, 0.02, 0.05, 0.1, 0.2, 0.5, 1, 2, 5, 10, 20, 50, 100, 200, 500, 1000, 5000 and 10,000 ng/mL. Lastly, we determined the metabolite contents by comparing the standard curves with the integrated peak areas.

Bioinformatics analysis

A fold-change cutoff of ≥ 2.0-fold change (upregulation greater than 2.0 times or downregulation less than 0.50 times) was used to identify differentially expressed proteins (DEPs) with a P value < 0.05. The normalized DEPs were subjected to cluster analysis via the R package version 3.4. Blast2GO (https://www.blast2go.com/) and the KEGG Automatic Annotation Server (KAAS) were used for GO annotation and KEGG pathway analysis of the target proteins. GO annotation and KEGG pathway enrichment analysis were performed via Fisher's exact test.

Conclusions

We analyzed proteomic changes at different time points during fruit development in the Korla balsam pear and identified 3762 DEPs in the Korla fragrant pear at three fruit development stages that are involved primarily in flavonoid biosynthesis, starch, sucrose, fructose, mannose, galactose and organic acid metabolism. The expression of proteins related to sugar metabolism and accumulation increased with increasing fruit development stage, which was consistent with the trend in soluble sugar content during fruit development. All 5 disaccharides, namely cellobiose, lactose, maltose, trehalose and sucrose, detected in this study were present at low levels in the early stages of fruit development but accumulated in large amounts from 15 to 20 WAF, which may explain the relatively high sweetness of the ripe Korla fragrant pear. In addition, the expression levels of proteins related to organic acid metabolism were consistent with the trend in organic acid content detected by UPLC-ESI-MS during fruit development. The contents of 34 organic acids are low in ripe Korla fragrant pear, and the ripe pear fruits used for consumption contain nine organic acids: 2-hydroxyphenylacetic acid, homovanillic acid, pyruvic acid, cis-aconitic acid, 3-methyladipic acid, hydroxyphenyllactic acid, taurine, fumaric acid and tartaric acid. The results provide valuable information for elucidating the molecular mechanisms underlying the high sweetness and low organic acidity of Korla fragrant pear, but further investigations are needed to evaluate their functional relevance to fruit quality in Korla fragrant pear.

Data availability

The mass spectrometry proteomics data have been deposited to the ProteomeXchange Consortium via the iProX partner repository with the Project ID, IPX0009417001.

Received: 25 July 2024; Accepted: 19 May 2025
Published online: 24 July 2025

References

1. Sato, Y. et al. Collaborative research project on conservation of fruit tree genetic resources in Xinjiang Uygur autonomous district of China. In *Annual Report on Exploration and Sintroduction of Plant Genetic Resources, vol. 24* 137–151 (2007).
2. Gong, X. et al. Candidate proteins involved in the calyx abscission process of 'kuerlexiangli' (*Pyrus sinkiangensis* Yu) identioned by iTRAQ analysis. *Acta Physiol. Plant.* **42**, 112 (2020).
3. Li, X., Li, X., Wang, T. & Gao, W. Chapter 24 – Nutritional composition of Pear cultivars (*Pyrus* spp.). In *Nutr. Compos. Fruit Cultiv.* (eds. Simmonds, M. S. J. & Preedy V. R.) (AcademicPress, 2016).
4. Yu, Y., Zhang, Q., Huang, J., Zhu, J. & Liu, J. Nondestructive determination of SSC in Korla fragrant Pear using a portable near-infrared spectroscopy system. *INFRARED PHYS. TECHN.* **116**, 103785 (2021).
5. Wang, Y., Mao, H., Lv, Y., Chen, G. & Jiang, Y. Comparative analysis of total wax content, chemical composition and crystal morphology of cuticular wax in Korla Pear under different relative humidity of storage. *Food Chem.* **339**, 128097 (2020).
6. Qi, X. et al. Identifying the candidate genes involved in the calyx abscission process of 'kuerlexiangli' (*Pyrus sinkiangensis* Yu) by digital transcript abundance measurements. *BMC Genom.* **14**, 727 (2013).
7. Yao, G. et al. Characteristics of components and contents of soluble sugars in Pear fruits from different species. *Scientia Agricultura Sinica*. **43**, 4229–4237 (2010).
8. Jiang, W. et al. Changes in the metabolome and nutritional quality of pulp from three types of Korla fragrant Pears with different appearances as revealed by widely targeted metabolomics. *Plants* **12**, 3981 (2023).
9. Chen, Y. et al. Comparison of fruit development dynamics and quality of Korla Balsam Pear and its different shoot transformation types. *Xinjiang Agricultural Sci.* **5**, 817–823 (2014).

10. Lan, H. P. et al. Quantitative evaluation method for ripeness of Korla fragrant Pear. *J. Agricultural Eng.* **5**, 325–330 (2015).
11. Xu, J. et al. Integrative analyses of widely targeted metabolic profiling and transcriptome data reveals molecular insight into metabolomic variations during Apple (*Malus domestica*) fruit development and ripening. *Int. J. Mol. Sci.* **21**, 4797 (2020).
12. Tao, S., Khanizadeh, S., Zhang, H. & Zhang, S. Anatomy, ultrastructure and lignin distribution of stone cells in two Pyrus species. *Plant. Sci.* **176**, 413–419 (2009).
13. Mamat, A. et al. Integrated transcriptomic and proteomic analysis reveals the complex molecular mechanisms underlying stone cell formation in Korla Pear. *Sci. Rep.* **11**, 7688 (2021).
14. Pan, Y. et al. Metabolic profiles of sugar metabolism and respiratory metabolism of Korla Pear (*Pyrus sinkiangensis* Yu) throughout fruit development and ripening. *Sci. Agricult. Sin.* **49**, 3391–3412 (2016).
15. Wu, J. et al. Variation of organic acids in mature fruits of 193 Pear (Pyrus spp.) cultivars. *J. Food Compos. Anal.* **109**, 104483 (2022).
16. Yamada, K. et al. Cloning of two isoforms of soluble acid invertase of Japanese Pear and their expression during fruit development. *J. Plant. Physiol.* **164**, 746–755 (2007).
17. Shen, C. et al. The change in microstructure of petioles and peduncles and transporter gene expression by potassium influences the distribution of nutrients and sugars in Pear leaves and fruit. *J. Plant. Physiol.* **232**, 320–333 (2019).
18. Lu, X., Liu, Y., An, J., Hu, H. & Peng, S. Isolation of a cinnamoyl coa reductase gene involved in formation of stone cells in Pear (*Pyrus pyrifolia*). *Acta Physiol. Plant.* **33**, 585–591 (2011).
19. Itai, A. et al. Identification of 1-aminocyclopropane-1-carboxylic acid synthase genes controlling the ethylene level of ripening fruit in Japanese Pear (*Pyrus pyrifolia* Nakai). *Mol. Gen. Genet.* **261**, 42–49 (1999).
20. Palma, J. M., Corpas, F. J. & Del Río L.A. Proteomics as an approach to the Understanding of the molecular physiology of fruit development and ripening. *J. Proteom.* **74**, 1230–1243 (2011).
21. Li, C., Chen, S. & Wang, Y. Physiological and proteomic changes of *Castanopsis fissa* in response to drought stress. *Sci. Rep.* **13**, 12567 (2023).
22. Li, L. et al. Systematically quantitative proteomics and metabolite profiles offer insight into fruit ripening behavior in *Fragaria* × *Ananassa*. *RSC Adv.* **9**, 14093–14108 (2019).
23. Chin, C. F. et al. Comparative proteomic analysis on fruit ripening processes in two varieties of tropical Mango (*Mangifera indica*). *Protein J.* **38**, 704–715 (2019).
24. Kok, S. Y., Namasivayam, P., Ee, G. C. & Ong-Abdullah, M. Comparative proteomic analysis of oil palm (*Elaeis guineensis* Jacq.) during early fruit development. *J. Proteom.* **232**, 104052 (2021).
25. Yu, Y. et al. Quantitative transcriptomic and proteomic analysis of fruit development and ripening in watermelon (*Citrullus lanatus*). *Front. Plant. Sci.* **13**, 818392 (2022).
26. Jiang, B. et al. Comparative proteomic analysis provides novel insights into the regulation mechanism underlying Papaya (*Carica Papaya* L.) exocarp during fruit ripening process. *BMC Plant. Biol.* **19**, 238 (2019).
27. Li, M. et al. Proteomic analysis reveals dynamic regulation of fruit development and sugar and acid accumulation in Apple. *J. Exp. Bot.* **67**, 5145–5157 (2016).
28. Gao, Z. et al. Proteomic analysis of Pear (*Pyrus pyrifolia*) ripening process provides new evidence for the sugar/acid metabolism difference between core and mesocarp. *Proteomics* **16**, 3025–3041 (2016).
29. Ross, P. L. et al. Multiplexed protein quantitation in Saccharomyces cerevisiae using amine-reactive isobaric tagging reagents. *Mol. Cell. Proteom.* **3**, 1154–1169 (2004).
30. Wang, Y. et al. Physiological and proteomic analysis of seed germination under salt stress in mulberry. *Front. Biosci. (Landmark Ed).* **28**, 49 (2023).
31. Skirycz, A. & Fernie, A. R. Past accomplishments and future challenges of the multi-omics characterization of leaf growth. *Plant. Physiol.* **189**, 473–489 (2022).
32. You, S. et al. Evaluating the microstructure and physicochemical properties of 'korla' fragrant Pear disease caused by Alternaria alternata: Vis-NIR hyperspectral microscope imaging coupled with convolutional neural network. *POSTHARVEST BIOL. TEC.* **212**, 112913 (2024).
33. Jin, M. et al. Genome-wide analysis and expression pattern of the PIN gene family during Korla fragrant Pear calyx development. *Acta Physiol. Plant.* **44**, 55 (2022).
34. Wang, X. et al. Investigating the resistance responses to Alternaria brassicicola in 'korla' fragrant Pear fruit induced by a biocontrol strain Bacillus subtilis Y2. *Postharvest. Biol. Technol.* **199**, 112293 (2023).
35. Zhang, H., Su, Y., Yu, Q. & Qin, G. Quantitative proteomic analysis of Pear (*Pyrus pyrifolia* Cv. Hosui) flesh provides novel insights about development and quality characteristics of fruit. *Planta* **253**, 69 (2021).
36. Liu, Z. et al. Integrative transcriptome and proteome analysis identifies major metabolic pathways involved in pepper fruit development. *J. Proteome Res.* **18**, 982–994 (2019).
37. Olmedo, P. et al. Proteomic and metabolomic integration reveals the effects of pre-flowering cytokinin applications on central carbon metabolism in table grape berries. *Food Chem.* **411**, 135498 (2023).
38. Olmedo, P. et al. Proteomic and Low-Polar metabolite profiling reveal unique dynamics in fatty acid metabolism during flower and berry development of table grapes. *Int. J. Mol. Sci.* **24**, 15360 (2023).
39. Pan, X. et al. iTRAQ protein profile analysis of tomato green-ripe mutant reveals new aspects critical for fruit ripening. *J. Proteome Res.* **13**, 1979–1993 (2014).
40. Jiao, Y., Zhang, J. & Pan, C. Integrated physiological, proteomic, and metabolomic analyses of Pecan cultivar 'pawnee' adaptation to salt stress. *Sci. Rep.* **12**, 1841 (2022).
41. Datir, S. & Regan, S. Advances in physiological, transcriptomic, proteomic, metabolomic, and molecular genetic approaches for enhancing Mango fruit quality. *J. Agric. Food Chem.* **71**, 20–34 (2023).
42. Lurie, S. Proteomic and metabolomic studies on chilling injury in Peach and nectarine. *Front. Plant. Sci.* **13**, 958312 (2022).
43. Li, X., Jiang, J., Chen, Z. & Jackson, A. Transcriptomic proteomic and metabolomic analysis of flavonoid biosynthesis during fruit maturation in *Rubus Chingii* Hu. *Front. Plant. Sci.* **12**, 706667 (2021).
44. Yadav, S. K., Kumar, V. & Singh, S. P. *Recent Trends and Techniques in Plant Metabolic Engineering* (Springer Nature, 2018).
45. Winkel-Shirley, B. Flavonoid biosynthesis. A colorful model for genetics, biochemistry, cell biology, and biotechnology. *Plant. Physiol.* **126**, 485–493 (2001).
46. Brunetti, C., Fini, A., Sebastiani, F., Gori, A. & Tattini, M. Modulation of phytohormone signaling: a primary function of flavonoids in plant–environment interactions. *Front. Plant. Sci.* **9**, 1042 (2018).
47. Vanholme, R., Meester, D. B., Ralph, J. & Boerjan, W. Lignin biosynthesis and its integration into metabolism. *Curr. Opin. Biotechnol.* **56**, 230–239 (2019).
48. Wang, L. et al. Transgenic expression of Flavanone 3-hydroxylase redirects flavonoid biosynthesis and alleviates anthracnose susceptibility in sorghum. *Plant. Biotechnol. J.* **18**, 2170–2172 (2020).
49. Wang, A. et al. A sweet potato cinnamate 4-hydroxylase gene, IbC4H, increases phenolics content and enhances drought tolerance in tobacco. *Acta Physiol. Plant.* **39**, 276 (2017).
50. Li, G. et al. Cloning and functional characterization of two cinnamate 4-hydroxylase genes from *Pyrus bretschneideri*. *Plant. Physiol. Biochem.* **156**, 135–145 (2020).
51. Guo, F., Wang, X., Liu, X., Xia, H. & Wang, X. Metabolic regulation of plants anthocyanin. *Chin. Bull. Life Sci.* **23**, 938–944 (2011).
52. Song, X. et al. Molecular cloning and identification of a Flavanone 3-hydroxylase gene from *Lycium chinense*, and its overexpression enhances drought stress in tobacco. *Plant. Physiol. Biochem.* **98**, 89–100 (2016).

53. Sarma, B., Das, K. & Bora, S. S. Physiology of fruit development. *Int. J. Curr. Microbiol. Appl. Sci.* **9**, 504–521 (2020).
54. Jiang, F. et al. RNAi-Mediated Silencing of the Flavanone 3-Hydroxylase gene and its effect on flavonoid biosynthesis in strawberry fruit. *J. PLANT. GROWTH REGUL.* **32**, 182–190 (2012).
55. Patrick, J. W., Botha, F. C. & Birch, R. G. Metabolic engineering of sugars and simple sugar derivatives in plants. *Plant. Biotechnol. J.* **11**, 142–156 (2013).
56. Schmölzer, K., Gutmann, A., Diricks, M., Desmet, T. & Nidetzky, B. Sucrose synthase: a unique glycosyltransferase for biocatalytic glycosylation process development. *Biotechnol. Adv.* **34**, 88–111 (2016).
57. Stein, O. & Granot, D. An overview of sucrose synthases in plants. *Front. Plant. Sci.* **10**, 95 (2019).
58. Braun, D. M., Wang, L. & Ruan, Y. L. Understanding and manipulating sucrose phloem loading, unloading, metabolism, and signalling to enhance crop yield and food security. *J. Exp. Bot.* **65**, 1713–1735 (2014).
59. Lv, G. et al. Molecular characterization, gene evolution, and expression analysis of the Fructose-1, 6-bisphosphate aldolase (FBA) gene family in wheat (*Triticum aestivum* L). *Front. Plant. Sci.* **8**, 1030 (2017).
60. Jedrzejczak-Krzepkowska, M., Kalinowska, H. & Bielecki, S. Beta-fruktofuranozydaza--właściwości, struktura i Zastosowanie [Beta-fructofuranosidase--properties, structure and applications]. *Postepy Biochem.* **57**, 401–410 (2011).
61. Chen, W. H. et al. Isolation,structural properties, bioactivities of polysaccharides from Dendrobium officinale Kimura et. Migo: a review. *Int. J. Biol. Macromol.* **184**, 1000–1013 (2021).
62. Caballero, B. *Encyclopedia of Food Sciences and Nutrition (Second Edition)* (Academic Press, 2003).
63. Yin, H. et al. Profiling of soluble sugar compositions in mature fruits of a diverse Pear (*Pyrus* spp.) germplasm by UPLC. *J. FOOD COMPOS. ANAL.* **132**, 106281. https://doi.org/10.1016/j.jfca.2024.106281 (2024).
64. Lü, J., Tao, X., Yao, G., Zhang, S. & Zhang, H. Transcriptome analysis of Low- and High-Sucrose Pear cultivars identifies key regulators of sucrose biosynthesis in fruits. *Plant. Cell. Physiol.* **61**, 1493–1506 (2020).
65. Mao, Y., Tian, S., Qin, Y. & Han, J. A new sensory sweetness definition and sweetness conversion method of five natural sugars, based on the Weber-Fechner law. *Food Chem.* **281**, 78–84 (2019).
66. Qi, X. & Tester, R. F. Fructose, galactose and glucose - In health and disease. *Clin. Nutr. ESPEN.* **33**, 18–28 (2019).
67. Vaclavik, V. A., Christian, E. W., Sugars, Vaclavik, V. A. & Christian, E. W. Sweeteners, and confections. In *Essentials of Food Science* (Springer,2014).
68. Pullicin, A. J., Penner, M. H. & Lim, J. The sweet taste of acarbose and maltotriose: relative detection and underlying mechanism. *Chem. Senses.* **44**, 123–128 (2019).
69. Dwivedi, R. S. Molecular basis of sweetness, recent concepts, an ideal sweetener and saccharide and non-saccharide sweet principles qualifying It. In *Alternative Sweet and Supersweet Principles* (ed. Dwivedi, R. S.) (Springer, 2022).
70. Huang, X., Wang, C., Zhao, Y., Sun, C. & Hu, D. Mechanisms and regulation of organic acid accumulation in plant vacuoles. *Hortic. Res.* **8**, 227 (2021).
71. Chandrasekhar, K. et al. Insight to the interaction of the Dihydrolipoamide acetyltransferase (E2) core with the peripheral components in the Escherichia coli pyruvate dehydrogenase complex via multifaceted structural approaches. *J. Biol. Chem.* **288**, 15402–15417 (2013).
72. Li, Y. et al.. Recent advances in pyruvate dehydrogenase kinase inhibitors: structures, inhibitory mechanisms and biological activities. *Bioorg. Chem.* **2024**, 107160 (2024).
73. Walker, R. P., Chen, Z. H. & Famiani, F. Gluconeogenesis in plants: a key interface between organic acid/amino acid/lipid and sugar metabolism. *Molecules* **26** (17), 5129 (2021).
74. Huang, S., Braun, H. P., Gawryluk, R. M. R. & Millar, A. H. Mitochondrial complex II of plants: subunit composition, assembly, and function in respiration and signaling. *Plant. J.* **98**, 405–417 (2019).
75. Gray, M. W. et al. The draft nuclear genome sequence and predicted mitochondrial proteome of Andalucia Godoyi, a protist with the most gene-rich and bacteria-like mitochondrial genome. *BMC Biol.* **18**, 22 (2020).
76. Shlizerman, L., Marsh, K., Blumwald, E. & Sadka, A. Iron-shortage-induced increase in citric acid content and reduction of cytosolic aconitase activity in Citrus fruit vesicles and calli. *Physiol. Plant.* **131**, 72–79 (2007).
77. Terol, J., Soler, G., Talon, M. & Cercos, M. The aconitate hydratase family from Citrus. *BMC Plant. Biol.* **10**, 222 (2010).
78. Martínez-Rivas, J. M. & Vega, J. M. Effect of culture conditions on the isocitrate dehydrogenase and isocitrate lyase activities in *Chlamydomonas reinhardtii*. *Physiol. Plant.* **88**, 599–603 (1993).
79. Sztrum, A. A., Sabatini, S. E. & Rodriguez, M. C. Isocitrate lyase activity and antioxidant responses in copper-stressed cultures of *Chlamydomonas reinhardtii* (Volvocales, Chlorophyceae). *PHYCOLOGIA* **51**, 135–143 (2012).
80. Shuab, R., Lone, R. & Koul, K. K. Cinnamate and cinnamate derivatives in plants. *Acta Physiol. Plant.* **38**, 64. https://doi.org/10.1007/s11738-016-2076-z (2016).
81. Zhang, S. *Pear Science* (China Agriculture Press, 2013).
82. Umer, M. J. et al. Identification of key gene networks controlling organic acid and sugar metabolism during watermelon fruit development by integrating metabolic phenotypes and gene expression profiles. *Hortic. Res.* **7**, 193 (2020).
83. Wang, Y. et al. Integrated transcriptomic and metabolomic analyses elucidate the mechanism of flavonoid biosynthesis in the regulation of mulberry seed germination under salt stress. *BMC Plant Biol.* **24** (1), 132 (2024).
84. Xu, J. D. et al. Integrative analyses of widely targeted metabolic profiling and transcriptome data reveals molecular insight into metabolomic variations during Apple (*Malus domestica*) fruit development and ripening. *Int. J. Mol. Sci.* **21** (13), 4797 (2020).

Author contributions

Conceptualization, Y.W., Q.Z., Q.C. and P.Y.; methodology, P.Y.; software, Q.Z.; validation, Z.W.; investigation, Y.D., W.J., L.M.; data curation, W.J., L.M., Y.D. and Z.W.; writing—original draft preparation, Y.W. and Q.C.; writing—review and editing, Y.D. and Y.W.; project administration, funding acquisition, Q.Z., P.Y. and Q.C. All authors have read and agreed to the published version of the manuscript.

Funding

This research was supported by the Corps of Agricultural Science and Technology Innovation Special Project (NCG202312) and the Corps Key Laboratory of Korla Fragrant Pear Germplasm Innovation, Quality Improvement and Efficiency Enhancement (2020DA004).

Competing interests

The authors declare no competing interests.

Ethics approval and consent to participate

The experimental research and field studies on plants in this work comply with the IUCN Policy Statement on Research Involving Species at Risk of Extinction and the Convention on the Trade in Endangered Species of

Wild Fauna and Flora. The experimental research on the plants in this study, including the collection of plant material, complies with relevant institutional, national, and international guidelines and legislation. Permission to collect *Pyrus sinkiangensis* Yü fruit was obtained, and the plant samples were located at the Xinjiang Academy of Agricultural Sciences, under voucher number PE 01828889.

Additional information

Supplementary Information The online version contains supplementary material available at https://doi.org/10.1038/s41598-025-03117-1.

Correspondence and requests for materials should be addressed to Y.W., P.Y. or Q.C.

Reprints and permissions information is available at www.nature.com/reprints.

Publisher's note Springer Nature remains neutral with regard to jurisdictional claims in published maps and institutional affiliations.